CODEN:LUTEDX/(TEAT-7115)/1-36/(2003)

Retrofocusing of Acoustic Wave Fields by Iterated Time Reversal

B. Lars G. Jonsson, Mats Gustafsson, Vaughan H. Weston, and Maarten V. de Hoop

Department of Electroscience
Electromagnetic Theory
Lund Institute of Technology
Sweden

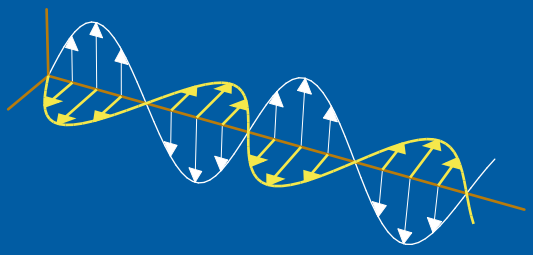

B. Lars G. Jonsson
ljonsson@math.toronto.edu

Department of Mathematics
Toronto University
Toronto, Ontario
Canada M5S 3G3
and
Electromagnetic Theory
The Alfvén Laboratory
Royal Institute of Technology
SE-100 44 Stockholm
Sweden

Mats Gustafsson
mats@es.lth.se

Department of Electroscience
Electromagnetic Theory
Lund Institute of Technology
P.O. Box 118
SE-221 00 Lund
Sweden

Vaughan H. Weston

Department of Mathematics
Purdue University
West Lafayette, IN47907-1395
USA

Maarten V. de Hoop
mdehoop@mines.edu

Center for Wave Phenomena
Colorado School of Mines
Golden, CO 80401
USA

Editor: Gerhard Kristensson

This series is divergent, therefore we
may be able to do something with it.
Oliver Heaviside

Nature laughs at the difficulties of integration.
Pierre-Simon Laplace

Abstract

In the present paper an iterative time-reversal algorithm, that retrofocuses an acoustic wave field to its controllable part is established. For a fixed temporal support, *i.e.*, transducer excitation time, the algorithm generates an optimal retrofocusing in the least-squares sense. Thus the iterative time-reversal algorithm reduces the temporal support of the excitation from the requirement of negligible remaining energy to the requirement of controllability. The time-reversal retrofocusing is analyzed from a boundary control perspective where time reversal is used to steer the acoustic wave field towards a desired state. The wave field is controlled by transducers located at subsets of the boundary, *i.e.*, the controllable part of the boundary.

The time-reversal cavity and time-reversal mirror cases are analyzed. In the cavity case, the transducers generate a locally plane wave in the fundamental mode through a set of ducts. Numerical examples are given to illustrate the convergence of the iterative time-reversal algorithm. In the mirror case, a homogeneous half space is considered. For this case the analytic expression for the retrofocused wave field is given for finite temporal support. It is shown that the mirror case does not have the same degree of steering as the cavity case. It is also shown that the pressure can be perfectly retrofocused for infinite temporal support. Two examples are given that indicate that the influence of the evanescent part of the wave field is small.

1 Introduction

Time-reversal acoustics is based on recording the wave field by a set of transducers, time reversing the recorded signal, and retransmitting the result. The retransmitted wave field propagates back in the medium towards its source of origin [5, 9–11, 13]. In this paper, the time-reversal approach is analyzed from a boundary control perspective [2, 3] in which time reversal is used to steer the acoustic wave field towards a desired state, corresponding to the original state. The boundary is divided into a controllable and an uncontrollable part. On the controllable part of the boundary, transducers are used to record or generate the acoustic wave field. The uncontrollable part of the boundary is acoustically hard [25].

Both the time-reversal cavity and the time-reversal mirror have been extensively studied by M. Fink *et al.*, see *e.g.*, [5, 9–11, 13]. The cavity and mirror cases describe measurement situations with transducers surrounding the original

source and only occupying a limited angular area, respectively. Applications of time-reversal algorithms include lithotripsy, pulse focusing, medical imaging, inverse scattering [10, 11], and optimal distinguishability measurements [6, 7]. The time-reversal approach gives a perfect retrofocusing if the transducers surround the original source, *i.e.*, the time reversal cavity, and the wave field is recorded until the wave field is quiescent, see *e.g.*, [2]. If the conditions for local energy decay are satisfied [1, 22], the retrofocusing error can be made arbitrary small as times approach infinity. An analysis of the super-resolving property of the time-reversal mirror is presented in [4].

From boundary control theory, it is known that transducers can steer the wave field towards an arbitrary field distribution if the region is controllable [3, 21]. If the configuration is not controllable an optimal control produces an optimal retrofocused wave field. The present paper establishes an iterative time-reversal algorithm that retrofocuses an acoustic wave field to its controllable part. The obtained iterative time-reversal algorithm reduces the temporal support of the transducer excitation from the requirement of negligible remaining energy to the requirement of controllability. In particular for a fixed temporal support of the excitation, the algorithm generates an optimal retrofocusing in the least-squares sense. The characteristics of the transducers are included. The considered cavity is a bounded domain with a perforated acoustically-hard boundary. Transducers induce the wave field through the fundamental (or plane wave) mode in a set of ducts [25]. Numerical examples are given to illustrate the convergence of the iterative time-reversal algorithm.

In the mirror case, a homogeneous half space is considered. For this case, it is shown that the pressure can be perfectly retrofocused for infinite temporal support. For finite temporal support the algorithm gives an optimal control for the propagating part of the wave field. A closed-form representation for the retrofocused wave field, with finite temporally supported excitation, from an initial Dirac-pressure source is given. Its behavior in the long time limit is calculated. Two examples of retrofocusing of a pressure source are given and the influence of the evanescent part of the wave is discussed.

The optimal measurements [6, 7] are discussed in the sense of maximal measured least-squares distinguishability of a scattering operator relative to a reference scattering operator. The obtained algorithm is the limit of a renormalized-series of iterated time reversals. It is noted in [6] that the limit of this renormalized-series is a time-harmonic, frequency tuned wave form that is corresponding to the frequency such that the largest eigenvalue of the squared time-reversed reflection operator, attains it maximum in a given frequency interval. The algorithm in the present paper uses *the sum* of the iterated squared time-reversed response operators, to obtain the retrofocusing of an initial prescribed field. Thus the resulting input signal for retrofocusing has a multi-frequency content, as opposed to the proposed algorithms in [6, 7].

The present paper begins with a short discussion of the boundary control of acoustic wave fields. Transducers are introduced and their restrictions on the boundary conditions are analyzed. In Section 3, the sufficient conditions for optimal boundary control with respect to a least-squares measure is given. As the first

example we consider the case where the material parameters are unknown, see Section 4. In Section 5, a cavity with acoustically hard walls and attached ducts is analyzed. Numerical examples are given. The time-reversal algorithm is shown to efficiently retrofocus the field of a initial pulse source. In Section 6, the mirror case is analyzed. The optimal control for measurements with negligible evanescent part is derived. For non-negligible evanescent part of the measured response, the closed-form expression for the time-reversal of an initial pressure source is derived. It is shown that for an initial pressure distribution, the evanescent part of the control have a marginal influence the resulting field, in the long excitation time limit. Section 7 is a discussion of the results.

2 The acoustic wave field and boundary control

2.1 The control state

In this section we state the acoustic equations, the boundary conditions and initial values assumed in the analysis. The goal is to focus the acoustic wave field to a desired state at a given finite time. To quantify the focusing, relative to the desired state, we use a weighted L^2 measure, in the form of an energy functional. We also introduce the boundary control, the admittance operator, a representation of the characteristics of a transducer, and the response operator due to a boundary control.

The control state is an acoustic wave field in the domain $\Omega \in \mathbb{R}^3$ and time interval $[0, T]$. The boundary of the domain, $\partial\Omega$, is assumed to be piecewise C^1, and thus the normal to the boundary is well defined almost everywhere. At the open subset $\Gamma_{\mathrm{t}} \subset \partial\Omega$ we have a set of transducers that are used to generate an acoustic wave field in the domain. The control state at time t is represented by the pressure, $p = p(\boldsymbol{x}, t)$, and the particle velocity, $\boldsymbol{v} = \boldsymbol{v}(\boldsymbol{x}, t)$. Given a desired final state, $\{p_T, \boldsymbol{v}_T\}$, we quantize the degree of focusing between the obtained control state at time T, $\{p(\cdot, T), \boldsymbol{v}(\cdot, T)\}$, and the desired state, with the weighted L^2-functional

$$\mathcal{J} = \frac{1}{2} \int_\Omega \left(\kappa(\boldsymbol{x}) |p(\boldsymbol{x}, T) - p_T(\boldsymbol{x})|^2 + \rho(\boldsymbol{x}) |\boldsymbol{v}(\boldsymbol{x}, T) - \boldsymbol{v}_T(\boldsymbol{x})|^2 \right) \mathrm{dV}(\boldsymbol{x}) \,. \tag{2.1}$$

The control state $\{p, \boldsymbol{v}\}$ satisfies the source-free acoustic equations

$$\begin{cases} \kappa(\boldsymbol{x}) \partial_t p + \nabla \cdot \boldsymbol{v} = 0 \\ \rho(\boldsymbol{x}) \partial_t \boldsymbol{v} + \nabla p = \boldsymbol{0} \end{cases} \qquad \text{for } \boldsymbol{x} \in \Omega \,, \text{ and } t \in [0, T] \,, \tag{2.2}$$

where the compressibility $\kappa(\boldsymbol{x})$ and the density $\rho(\boldsymbol{x})$ model the interaction between the acoustic wave field and the material. It is assumed that material parameters κ and ρ are positive and belong to $\mathrm{L}^\infty(\Omega)$, *i.e.*, the parameters are bounded and measurable. In the process of retrofocusing we assume the initial conditions

$$p(\boldsymbol{x}, 0) = 0 \quad \text{and } \boldsymbol{v}(\boldsymbol{x}, 0) = \boldsymbol{0} \quad \text{for } \boldsymbol{x} \in \Omega \,. \tag{2.3}$$

In our model the transducers are supported on the controllable part Γ_{t} of the boundary. Given a boundary control [21], $p_+ = p_+(\boldsymbol{x}, t)$, $\boldsymbol{x} \in \Gamma_{\mathrm{t}}$ the characteristics of the

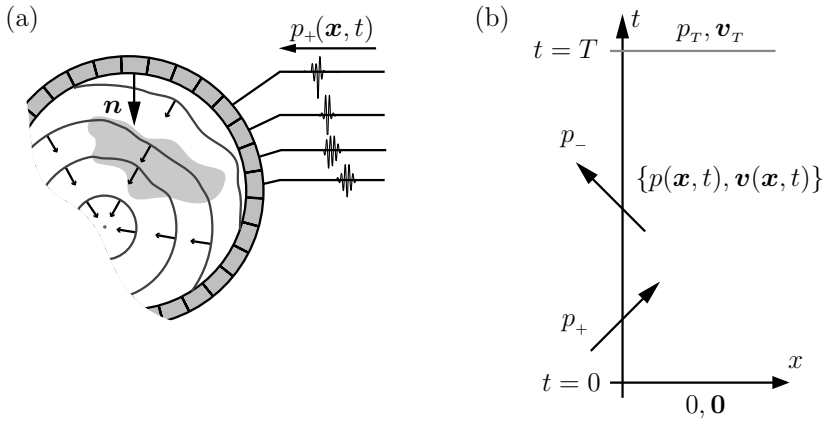

Figure 1: The control state: The boundary control p_+ is prescribed at the boundary, given quiescent initial condition, we measure the response p_-. The desired final state $\{p_T, \boldsymbol{v}_T\}$ is shown as the state at time $t = T$ in Figure (b).

transducers determine how the field is induced in the domain. Here, we model the transducer characteristic with the transducer's admittance operator $\mathcal{Y}$, that maps its domain $\mathcal{D} \subset \mathrm{L}^2$ to L^2, and is invertible. Thus the boundary condition at the controllable part of the boundary, see Figure 1, takes the form,

$$\frac{(\mathcal{Y}p)(\boldsymbol{x},t) + v_{\mathrm{n}}(\boldsymbol{x},t)}{2} = p_+(\boldsymbol{x},t) \quad \text{for } \boldsymbol{x} \in \Gamma_{\mathrm{t}} \ , \ \text{and } t \in [0,T] \ , \tag{2.4}$$

where v_{n} is the normal component of the particle velocity, *i.e.*, $v_{\mathrm{n}} = \boldsymbol{v} \cdot \boldsymbol{n}$ and $\boldsymbol{n}$ is the inward unit normal vector to the boundary, see Figure 1a. The boundary condition above, is said to be in the velocity normalization [16–18].

The uncontrollable part of the boundary, $\Gamma_{\mathrm{w}} = \partial\Omega \setminus \Gamma_{\mathrm{t}}$ (the 'wall'), is made of a particular material with characteristics $\mathcal{U}$ giving the boundary condition

$$(\mathcal{U}p)(\boldsymbol{x},t) + v_{\mathrm{n}}(\boldsymbol{x},t) = 0 \quad \text{for } \boldsymbol{x} \in \Gamma_{\mathrm{w}} \ \text{ and } t \in [0,T] \ . \tag{2.5}$$

Here, $\mathcal{U}$ is a continuous mapping from L^2 to L^2.

The operators $\mathcal{Y}$ and $\mathcal{U}$ are chosen such that they admit only ingoing wave constituents and such that the problem of solving the acoustic wave equation is well posed with this boundary condition, see Ref. 19. Observe that $\mathcal{U} = 0$ in (2.5) corresponds to an acoustically hard (uncontrolable) boundary. The case with $\mathcal{Y} = 1$ in (2.4) represents boundary conditions in the form of a locally plane wave propagating inward into the domain *i.e.*, in the $\boldsymbol{n}$-direction [25].

We assume that the transducers can also be used as receivers, and measuring the outgoing field component, p_-, at the boundary, see Figure 1b. This component is given by

$$p_-(\boldsymbol{x},t) = \frac{(\mathcal{Y}p)(\boldsymbol{x},t) - v_{\mathrm{n}}(\boldsymbol{x},t)}{2} \quad \text{for } \boldsymbol{x} \in \Gamma_{\mathrm{t}} \ \text{ and } t \in [0,T] \ . \tag{2.6}$$

The relation between the boundary control p_+ and the measured outgoing field component p_-, for zero initial conditions, is the response operator $\mathcal{R}$, which is also

called scattering operator or reflection operator *e.g.*, [6, 7],

$$p_-(\boldsymbol{x},t) = (\mathcal{R}p_+)(\boldsymbol{x},t) \quad \text{for } \boldsymbol{x} \in \Gamma_{\mathrm{t}} \text{ and } t \in [0,T] \,. \tag{2.7}$$

Given a boundary control, we assume that we can obtain its response either by measurements on the domain, *i.e.*, using the transducers to measure the response to the given boundary control, or by simulation, given that the density and the compressibility in Ω

In our formulation the boundary control is not uniquely determined. There are many acoustic wave field configurations where it is clear that several boundary controls minimize $\mathcal{J}$, *e.g.*, a homogeneous slab with excitation times that allows the wave field to pass through the slab.

2.2 The observation states

In this section, we define the notion of initial observation, an observation, and observation state. The observation of an observation state is used in constructing the boundary control for the control state.

To distinguish between the control states and the field used for observation, we introduce the notation $\{q(\boldsymbol{x},t), \boldsymbol{u}(\boldsymbol{x},t)\}$ for the observation state at times $t \in [-T,0]$. The observation state $\{q, \boldsymbol{u}\}$ solves (2.2) and for convenience we let the observation take place in the time interval $[-T,0]$.

We define the initial observation state through its initial conditions

$$q(\boldsymbol{x},-T) = p_T(\boldsymbol{x}) \quad \text{and} \quad \boldsymbol{u}(\boldsymbol{x},-T) = -\boldsymbol{v}_T(\boldsymbol{x}) \quad \text{for } \boldsymbol{x} \in \Omega \,. \tag{2.8}$$

The observation of the initial observation state is carried out with the receivers coinciding with the transducers for the control state, *i.e.*, the measurement in terms of the field at the boundary is

$$q_-(\boldsymbol{x},t) = \frac{(\mathcal{Y}q)(\boldsymbol{x},t) - u_{\mathrm{n}}(\boldsymbol{x},t)}{2} \quad \text{for } \boldsymbol{x} \in \Gamma_{\mathrm{t}} \text{ and } t \in [-T,0] \,. \tag{2.9}$$

Consequently, the boundary condition for the controllable part of the boundary takes the form

$$\frac{(\mathcal{Y}q)(\boldsymbol{x},t) + u_{\mathrm{n}}(\boldsymbol{x},t)}{2} = q_+ \quad \text{for } \boldsymbol{x} \in \Gamma_{\mathrm{t}} \text{ and } t \in [-T,0] \,. \tag{2.10}$$

The initial observation is thus given by $q_-^{(0)} = q_-$ setting $q_+ = 0$ in (2.10). On the uncontrollable part of the boundary, the field satisfies the boundary condition (*cf.* (2.5))

$$(\mathcal{U}q)(\boldsymbol{x},t) + u_{\mathrm{n}}(\boldsymbol{x},t) = 0 \quad \text{for } \boldsymbol{x} \in \Gamma_{\mathrm{w}} \text{ and } t \in [-T,0] \,. \tag{2.11}$$

The relation between q_- and q_+ and the initial conditions are, by the superposition principle

$$q_-(\boldsymbol{x},t) = (\mathcal{R}q_+)(\boldsymbol{x},t) + q_-^{(0)}(\boldsymbol{x},t) \quad \text{for } \boldsymbol{x} \in \Gamma_{\mathrm{t}} \text{ and } t \in [-T,0] \,, \tag{2.12}$$

where $\mathcal{R}$ coincide with the $\mathcal{R}$ in (2.7) since q_- and p_- are both the measured response with the same receivers of the acoustic wave equations with identical domain and type of boundary conditions.

We consider only operators $\mathcal{Y}$ and $\mathcal{U}$ such that the initial boundary value problem (2.2), (2.8), (2.10)–(2.11) is well posed, *i.e.*, we do not admit boundary conditions that specify an out-going field, see Ref. 19.

With the above given information about the response operator and the initial observation, we will search for an optimal boundary control, *i.e.*, the control applied in (2.4) such that the resulting control state at time T minimizes the least-squares functional $\mathcal{J}$, see (2.1), for a given $\{p_T, \boldsymbol{v}_T\}$.

3 Retrofocusing by time reversal

The time-reversal operator $\mathcal{T}$ is defined as

$$(\mathcal{T}p)(\boldsymbol{x},t) = p(\boldsymbol{x},-t)\ . \tag{3.1}$$

If $\{p,\boldsymbol{v}\}$ solves the acoustic wave equation, (2.2), then so does $\{\mathcal{T}p,-\mathcal{T}\boldsymbol{v}\}$.

3.1 Energies

In this section, we define the energy corresponding to the acoustic wave field, and reformulate the least-squares functional $\mathcal{J}$ on the interior of the domain into a functional on the boundary.

The energy at time t of the observation state $\{q(\boldsymbol{x},t),\boldsymbol{u}(\boldsymbol{x},t)\}$ is defined by

$$E[q,\boldsymbol{u}](t) = \frac{1}{2}\int_\Omega \kappa(\boldsymbol{x})|q(\boldsymbol{x},t)|^2 + \rho(\boldsymbol{x})|\boldsymbol{u}(\boldsymbol{x},t)|^2\,\mathrm{dV}(\boldsymbol{x})\ . \tag{3.2}$$

The energy conservation is given as

$$E[q,\boldsymbol{u}](0) - E[q,\boldsymbol{u}](-T) = \int_{-T}^0\int_{\partial\Omega} q(\boldsymbol{x},t)u_{\mathrm{n}}(\boldsymbol{x},t)\,\mathrm{dS}(\boldsymbol{x})\,\mathrm{d}t\ , \tag{3.3}$$

by Gauss theorem with the direction of normal unit vector as in Figure 1a. Let $E_0 = E[q,\boldsymbol{u}](0)$ then, with initial conditions (2.3) and (2.8) and energy identities (3.2)–(3.3), we rewrite $\mathcal{J}$ according to

$$\mathcal{J} = E_0 + \int_0^T\int_{\partial\Omega}\big(p(\boldsymbol{x},t) - (\mathcal{T}q)(\boldsymbol{x},t)\big)\big(v_{\mathrm{n}}(\boldsymbol{x},t) + (\mathcal{T}u_{\mathrm{n}})(\boldsymbol{x},t)\big)\,\mathrm{dS}(\boldsymbol{x})\,\mathrm{d}t\ . \tag{3.4}$$

3.2 Controllability

In this section, we show that the uncontrollable subspace is orthogonal to the controllable subspace. Assumptions: for acoustically hard or soft uncontrollable boundaries, under conditions to be made precise below. We also introduce the concept of 'equal fields on the boundary'.

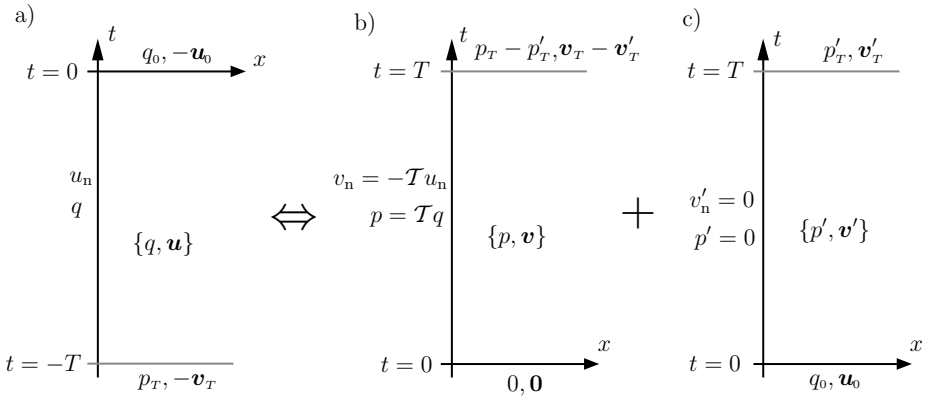

Figure 2: Controllable and uncontrollable subspaces for the equal fields on the boundary. Boundary fields such that $p = \mathcal{T} q$ and $v_\mathrm{n} = -\mathcal{T} u_\mathrm{n}$ decompose the original state into its controllable and uncontrollable part. a) In the observation state, the wave field is decomposed into the observed boundary field $\{q, u_\mathrm{n}\}$ and the non-observed remaining field $\{q_0, -\boldsymbol{v}_0\}$. b) In the control state, the boundary field (2.6) is time reversed and retransmitted into the region. c) The error term corresponds to the non-observable and non-controllable part of the wave field.

In general it is not possible to retrofocus the wave field to the desired wave field $\{p_T, \boldsymbol{v}_T\}$, at best the wave field retrofocuses to the controllable part of the wave field *i.e.*, to the part of $\{p_T, \boldsymbol{v}_T\}$ that is possible to reach from the boundary. This projection, to the controllable part, is achieved when the boundary fields are identical in the control and observation state *viz.*,

$$p = \mathcal{T} q \quad \text{and } v_\mathrm{n} = -\mathcal{T} u_\mathrm{n} \quad \text{when } \boldsymbol{x} \in \Gamma_\mathrm{t} \text{ and } t \in [0, T] \,. \tag{3.5}$$

This goal of retrofocusing cannot always be achieved. For an example, see Section 6. We denote the condition (3.5) as the 'equal fields on the boundary' condition. If the 'equal fields on the boundary' condition is achieved it gives a constructive description of the controllable, the uncontrollable, observable and unobservable parts of the wave field. Observe that it is not possible to enforce (3.5) for the acoustic wave equation together with arbitrary initial data. In general, on set of boundary condition (2.4) uniquely determines both the pressure and the particle velocity in the region. In this section we examine what the 'equal fields at the boundary' condition implies. In Section 3.3 it is shown that the time reversal approach can be used to achieve the 'equal field on the boundary' condition from well posed initial boundary value problems if the admittance operator commutes with the time reversal operator.

The observation (measurement) of the response of a boundary control p_+ and an initial state $\{p_0(\boldsymbol{x}), \boldsymbol{v}_0(\boldsymbol{x})\}$ is expressed as

$$p_- = \mathcal{R} p_+ + \mathcal{O}_{\Gamma_\mathrm{t}}(p_0, \boldsymbol{v}_0) \quad \text{for } \boldsymbol{x} \in \Gamma_\mathrm{t} \text{ and } t \in [0, T] \,, \tag{3.6}$$

where $\mathcal{O}_{\Gamma_\mathrm{t}}$ is an linear map from $\mathrm{L}^2(\Omega)$ to $\mathrm{L}^2(\Gamma_\mathrm{t} \times [0, T])$. The unobservable initial states N_Ω are defined as

$$\mathrm{N}_\Omega = \big\{ \{p_0, \boldsymbol{v}_0\} \in \mathrm{L}^2(\Omega) : \mathcal{O}_{\Gamma_\mathrm{t}}(p_0, \boldsymbol{v}_0) = 0 \in \mathrm{L}^2(\Gamma_\mathrm{t} \times [0, T]) \big\}, \tag{3.7}$$

i.e., they are the null space of $\mathcal{O}_{\Gamma_t}$, and thus a closed linear subspace of L^2_Ω. The observable initial states is the orthogonal complement to N_Ω, and $N^\perp_\Omega$ is a closed linear subspace of L^2_Ω, hence $L^2_\Omega = N_\Omega \oplus N^\perp_\Omega$. Solving the control problem (2.2)–(2.4) for some p_+, and its corresponding observation problem (2.2),(2.8),(2.10) and (2.11), for some q_+, gives the corresponding field $\{p, v_n\}$ and $\{q, u_n\}$ at the controllable boundary Γ_t. If this field for some given p_+, q_+ satisfy (3.5), then from the superposition principle, see Figure 2 we note that the controlable and uncontrollable part of the wave field coincide with the observable and unobservable. In the next section we derive a sufficient condition on the transducer admittance $\mathcal{Y}$ so that the 'equal field on the boundary' condition is achievable.

Now, since L^2_Ω is a Hilbert space with the κ, ρ-weighed standard inner product, the least-squares functional (2.1) is minimized by projecting the desired state on the controllable space, $N^\perp_\Omega$. This follows from the orthogonal projection theorem in Hilbert spaces, see *e.g.*, [24]. The final state $\{p_T - p'_T, \boldsymbol{v}_T - \boldsymbol{v}'_T\}$ is the controllable part of the original state $\{p_T, \boldsymbol{v}_T\}$. The error $\{p'_T, \boldsymbol{v}'_T\}$ is the uncontrollable (and unobserved) part of the original state. To show that the controllable and uncontrollable parts are orthogonal, in other words

$$\int_\Omega \kappa(\boldsymbol{x})\big(p_T(\boldsymbol{x}) - p'_T(\boldsymbol{x})\big)p'_T(\boldsymbol{x}) + \rho(\boldsymbol{x})\big(\boldsymbol{v}_T(\boldsymbol{x}) - \boldsymbol{v}'_T(\boldsymbol{x})\big) \cdot \boldsymbol{v}'_T(\boldsymbol{x})\,\mathrm{dV}(\boldsymbol{x}) = 0\ , \quad (3.8)$$

we use the energy estimates of the three problems depicted in Figure 2. Energy identities give, for an acoustically hard or soft uncontrollable part of the boundary,

$$E[p_T, \boldsymbol{v}_T] + \int_{-T}^{0}\int_{\Gamma_t} q u_n\,\mathrm{dS}\,\mathrm{d}t = E[q_0, \boldsymbol{u}_0]\ , \quad (3.9)$$

while

$$\int_0^T \int_{\Gamma_t} p v_n\,\mathrm{dS}\,\mathrm{d}t = E[p_T - p'_T, \boldsymbol{v}_T - \boldsymbol{v}'_T]\ , \quad (3.10)$$

and $E[q_0, \boldsymbol{u}_0] = E[p'_T, \boldsymbol{v}'_T]$. Upon combining these identities we obtain the orthogonality (3.8).

Thus if it is possible to generate 'equal fields on the boundary', we are able to reconstruct the controllable part of the final state $\{p_T - p'_T, \boldsymbol{v}_T - \boldsymbol{v}'_T\}$. We derive in the next section sufficient conditions for the fields on the boundary to be equal in the sense of (3.5).

3.3 Iterated time-reversal retrofocusing

In this section a well posed iterative algorithm is introduced to solve the condition of equal fields on the boundary, (3.5) for a class of transducer admittances.

Using a standard energy argument on Figure 2b, with either $p = \mathcal{T} q$ or $v_3 = -\mathcal{T} u_3$ for $x \in \Gamma_t$ and either acoustically soft, $p = 0$ or acoustically hard, $v_3 = 0$, for $x \in \Gamma_w$, the interior field is uniquely defined.

The equal boundary fields condition (3.5) can be rewritten in the observed quantities $\{p_-, q_-\}$, and the boundary controls $\{p_+, q_+\}$ using (2.4), (2.6), (2.9) and (2.10).

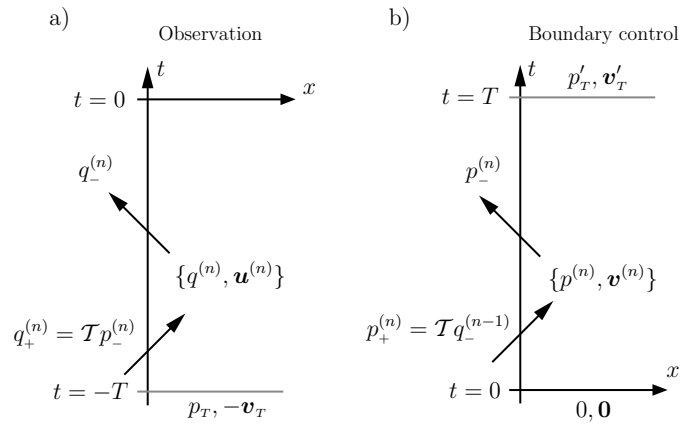

Figure 3: The iterated time-reversal algorithm. b) an observation $q_-^{(n-1)}$ is time reversed and used as a boundary control, to produce the output fields and the final state $\{p_T^{(n)}, \boldsymbol{v}_T^{(n)}\}$ and the output $p_-^{(n)}$. a) the output, $p_-^{(n)}$, is recorded, time reversed, and used as boundary control for the observation states, to produce the observation $q_-^{(n)}$, that, once again, is used to improve the final state.

We find

$$\begin{cases} \mathcal{Y}^{-1} p_+ + \mathcal{Y}^{-1} p_- = \mathcal{T}\mathcal{Y}^{-1} q_+ + \mathcal{T}\mathcal{Y}^{-1} q_- \ , \\ p_+ - p_- = -\mathcal{T} q_+ + \mathcal{T} q_- \ . \end{cases} \quad \boldsymbol{x} \in \Gamma_{\mathrm{t}} \ , \quad t \in [0, T]. \tag{3.11}$$

In terms of the response operator (2.12) we note that for a given boundary control q_+ and given initial observation, we have $q_- = \mathcal{R} q_+ + q_-^{(0)}$.

If (3.11) admits a solution, substituting the response operator, p_+ and q_+ satisfy the system

$$\begin{cases} p_+ = \frac{1}{2} \left(\mathcal{Y}\mathcal{T}\mathcal{Y}^{-1} + \mathcal{T} \right) \mathcal{R} q_+ + \frac{1}{2} \left(\mathcal{Y}\mathcal{T}\mathcal{Y}^{-1} - \mathcal{T} \right) q_+ + \frac{1}{2} \left(\mathcal{Y}\mathcal{T}\mathcal{Y}^{-1} + \mathcal{T} \right) q_-^{(0)} \ , \\ q_+ = \frac{1}{2} \left(\mathcal{Y}\mathcal{T}\mathcal{Y}^{-1} + \mathcal{T} \right) \mathcal{R} p_+ + \frac{1}{2} \left(\mathcal{Y}\mathcal{T}\mathcal{Y}^{-1} - \mathcal{T} \right) p_+ \ , \end{cases} \tag{3.12}$$

for $\boldsymbol{x} \in \Gamma_{\mathrm{t}}$ and $t \in [0, T]$. If the admittance commutes with the time reversal *i.e.*,

$$\mathcal{Y}\mathcal{T} = \mathcal{T}\mathcal{Y} \ , \tag{3.13}$$

as *e.g.*, for a constant admittance operator of a duct, see Section 5, then the requirement (3.12) simplifies to the linear system

$$\begin{cases} p_+ = \mathcal{T}\mathcal{R} q_+ + \mathcal{T} q_-^{(0)} \\ q_+ = \mathcal{T}\mathcal{R} p_+ \end{cases} \quad \text{or} \quad \begin{pmatrix} 1 & -\mathcal{T}\mathcal{R} \\ -\mathcal{T}\mathcal{R} & 1 \end{pmatrix} \begin{pmatrix} p_+ \\ q_+ \end{pmatrix} = \begin{pmatrix} \mathcal{T} q_-^{(0)} \\ 0 \end{pmatrix}. \tag{3.14}$$

This system can be solved in a variety of ways if the response operator $\mathcal{R}$ is known. In the case where only the action of $\mathcal{R}$ on an incident field is known, as in our case, the system is preferably solved by iterative methods. If $\mathcal{R}$ is sufficiently small, *i.e.*, the spectral radius of $\mathcal{R}$ in L^2 is smaller than 1, an iterative scheme of the Jacobi type iterations [28] converges. This gives the iterated time-reversal algorithm

$$\begin{cases} p_+^{(n)} = \mathcal{T}\mathcal{R} q_+^{(n-1)} = \mathcal{T} q_-^{(n-1)} \\ q_+^{(n)} = \mathcal{T}\mathcal{R} p_+^{(n)} = \mathcal{T} p_-^{(n)} \end{cases} \quad \text{for} \quad n = 1, 2, ... \tag{3.15}$$

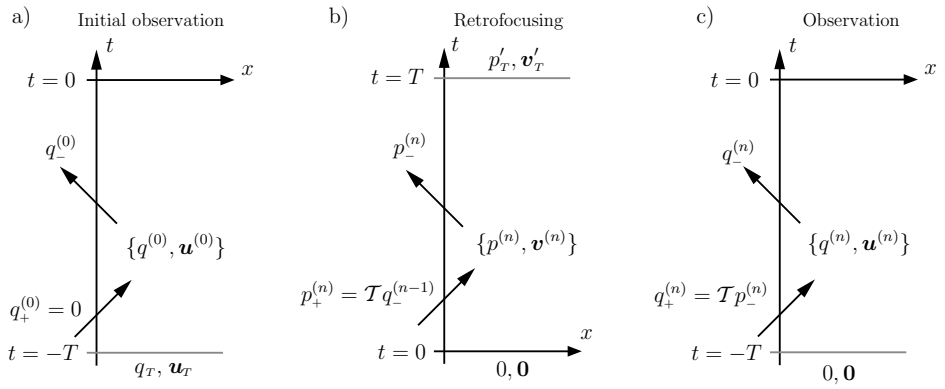

Figure 4: Iterated time-reversal retrofocusing. a) The output field is recorded from the original field as the initial observation or the initial step of the algorithm $n = 0$. b) in the retrofocusing, the recorded output $q_-^{(n\,-\,1)}$ is time reversed and re-emitted into the domain to produce the final state $\{p_T^{(n)}, -\boldsymbol{v}_T^{(n)}\}$ and the output $p_-^{(n)}$. c) in the observation, the output $p_-^{(n)}$ is time reversed and re-emitted into the domain to give the output $q_-^{(n)}$.

where $q_-^{(0)}$ is the initial measurement, see Figure 3 and Section 2.2. The boundary control and the final state are given by

$$p_+ = \sum_{n=1}^{\infty} p_+^{(n)} = \sum_{n=1}^{\infty} (\mathcal{T}\mathcal{R})^2 \mathcal{T} q_-^{(0)} \quad \text{and} \quad \{p_T, \boldsymbol{v}_T\} = \sum_{n=1}^{\infty} \{p_T^{(n)}, \boldsymbol{v}_T^{(n)}\}, \tag{3.16}$$

respectively. The iterated time-reversal algorithm (3.15) is initiated by recording the output field, $q_-^{(0)}$ generated by the original state $\{p_T, -\boldsymbol{v}_T\}$. This recorded output field is time reversed and re-emitted into the domain. Recording and time reversal of the corresponding output field iterates the algorithm.

4 Example: Time-reversal retrofocusing

In this section, the theory of Section 3 is applied to the problem of retrofocusing a wave field towards its initial state when both the initial state, and the material parameters of the object are unknown. This problem has been thoroughly analyzed by M. Fink *et al*, see *e.g.*, Refs [10–13]. In the time-reversal retrofocusing it is assumed that an initial state $\{q_T, \boldsymbol{u}_T\}$ exists in the object at time $t = -T$. This initial wave field is generated either by sources inside the object or by a field on the surface of the object.

The output $q_-^{(0)}$ is recorded at the boundary Γ_{t} for times $-T < t < 0$, see Figure 4a. This initial observed field is time reversed and re-emitted into the domain, see Figure 4b. The retrofocusing is carried out with the iterative time reversal algorithm (3.15). From Section 3, it is concluded that the final state $\{p'_T, -\boldsymbol{v}'_T\}$ coincides with the controllable part of the initial state, $\{q_T, \boldsymbol{u}_T\}$. Observe that the retrofocusing does not require knowledge of the initial state nor the material parameters.

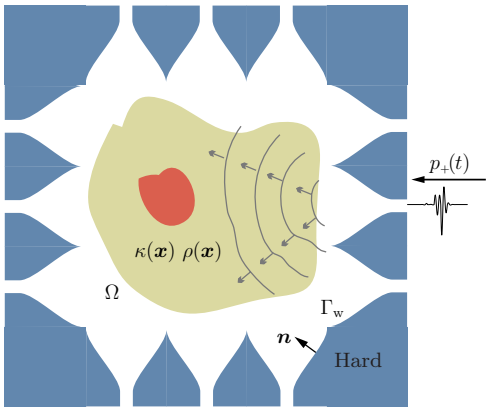

Figure 5: The cavity geometry. The boundary of the cavity is divided into the transducer surface, Γ_t, and the acoustically hard wall, Γ_w. The transducers induce the boundary control, $p_+(\boldsymbol{x}, t)$, as a locally plane wave propagating in the $\boldsymbol{n}$-direction, where $\boldsymbol{n}$ is the inward unit normal.

5 Example: Time-reversal cavity

5.1 Acoustically-hard boundary with ducts

In this section, the acoustically-hard boundary cavity is considered, with transducers and receivers in the form of narrow ducts. The particular form of the transducers and receivers corresponds to a simple admittance operator. We present a numerical simulation in three dimensions of the retrofocusing and the resulting fields.

The cavity is a bounded region with a perforated acoustically-hard boundary. The perforations are located in the end of a set of ducts. The wave field is induced through the perforations Γ_t, see Figure 5. If the ducts are sufficiently narrow and long, it is only the fundamental mode that propagates, *i.e.*, a locally plane wave, propagating in the $\boldsymbol{n}$-direction, see Ref 23, 25. In this case the admittance operator reduces to a scalar constant, *e.g.*, ,

$$\mathcal{Y} = \mathcal{Y}_0 = \sqrt{\kappa_0/\rho_0}\,. \tag{5.1}$$

The sufficient condition (3.13) of commutation between the admittance operator and the time reversal operator is trivially satisfied. Moreover, we consider only finite times, and hence the spectral radius of $\mathcal{R}$ is less than one. This is typical for finites time as some energy remains in the domain. The uncontrollable part of the boundary is acoustically hard, *i.e.*, $\mathcal{U} = 0$. For this case the iterated time reversal focusing algorithm (3.15) reduces to $p_+^{(\mathrm{n})} = \mathcal{T} q_-^{(\mathrm{n}-1)}$ and $q_+^{(\mathrm{n})} = \mathcal{T} p_-^{(\mathrm{n})}$.

5.2 Numerical results

To illustrate the iterated time reversal algorithm, a numerical example is presented. A cubic cavity with side length $L = 1$ and 4 horns attatched to each side is considered. The acoustic wave equation is solved with a standard Leap-Frog scheme,

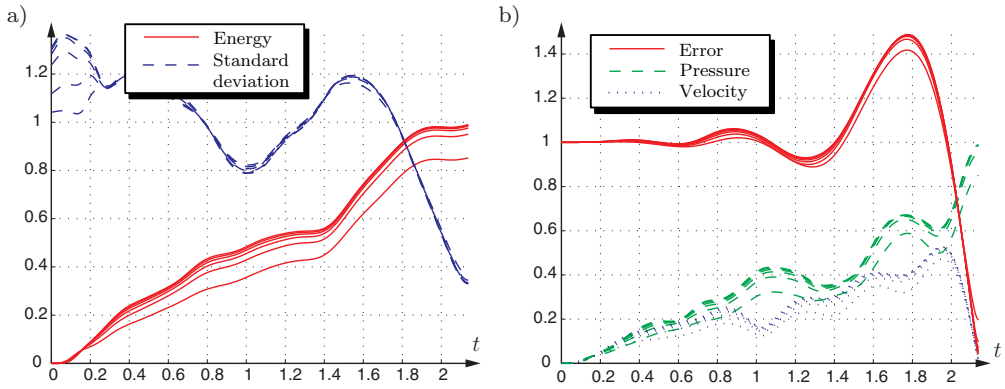

Figure 6: Example of a focused pressure in the cavity. Each improvement of the respective family of lines above is obtained by including one more term in the sum (3.16). a: the field energy is concentrated at $T = 2.2\,\mathrm{s}$. The standard deviation of the energy around its center point is minimized at the focusing time T. b: The error term is $\sqrt{\mathcal{J}}$. The pressure part of the energy dominates the velocity part at the focusing time T.

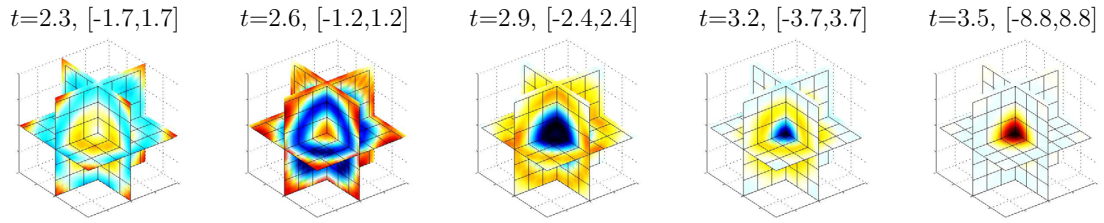

Figure 7: Example of a retrofocused pressure in the cavity; the range is given in the brackets. The focusing time is T=3.5.

where the cavity, the horns, and the ducts are discretized on an equidistant grid with discretization $L/82$. The fundamental mode is induced with a Huygens surface in the ducts and the ducts are terminated with a perfectly matched layer. The temporal step is chosen according to the CFL condition [30] to minimize the numerical dispersion.

In Figure 6a, the first two moments of the energy distribution is depicted. It is obvious that the field energy is concentrated around the focusing time $T = 2.2$. At these times the energy is centered around the focusing point. The concentration of the energy is measured with the variation of the energy. The variation is scaled such that an energy with uniform distribution has unit variation. From the variation curve, it is clear that the wave field is concentrated around the focusing point at the focusing time but the wave field is not concentrated for other times. The field energy of each field component is shown in Figure 6b. The retrofocused field for a case with retrofocusing at $T = 3.5$ is depicted in Figure 7

6 Example: Time-reversal mirror

For the time-reversal mirror, we consider the half space $\Omega = \{\boldsymbol{x} : x_3 \geq 0\}$, with homogeneous material parameters $\kappa = \kappa_0$ and $\rho = \rho_0$. The transducers are located at the plane $\Gamma_{\mathrm{t}} = \{\boldsymbol{x} \in \mathbb{R}^3 : \ x_3 = 0\}$. Thus we assume that the transducers can prescribe a boundary condition on the whole plane *cf.* (2.4).

6.1 The impedance operator

A non-reflective admittance operator [16, 17, 31, 32] is given here as an explicit integral representation, as well as its adjoint with respect to the standard L^2-inner product.

The characteristics of the transducers and receivers are modeled by the wave-splitting admittance operator, $\mathcal{Y}$, with symbol [8, 29]

$$\boldsymbol{y}(\tilde{\boldsymbol{\xi}}, s) = s^{-1}\sqrt{s^2\kappa_0\rho_0 + \tilde{\xi}^2}\ , \tag{6.1}$$

where s is the Laplace transform variable corresponding to time, and $\tilde{\boldsymbol{\xi}} = (\xi_1, \xi_2)$ the transverse Fourier variable corresponding to $\tilde{\boldsymbol{x}} = (x_1, x_2)$. We use the notation $\tilde{x} = |\tilde{\boldsymbol{x}}|$ and $\tilde{\xi} = |\tilde{\boldsymbol{\xi}}|$ to denote the norm of $\tilde{\boldsymbol{x}}$ and $\tilde{\boldsymbol{\xi}}$, respectively.

The above square root is taken with the branch-cut at the negative real axis, *i.e.*, $\sqrt{s^2} = s$, when $\operatorname{Re} s > 0$. An energy re-normalization of the field removes the constant material parameters in the acoustic wave equation (2.2) [14, p37], and consequently in (6.1). The inverse of the admittance, the impedance, satisfies the transform relation

$$\frac{s}{\sqrt{s^2 + \tilde{\xi}^2}} = \mathcal{L}\mathcal{F}\frac{\delta'(t - |\tilde{\boldsymbol{x}}|)}{2\pi|\tilde{\boldsymbol{x}}|}\ , \tag{6.2}$$

for $t \geq 0$. Here $\mathcal{L}$ denotes the Laplace transform and $\mathcal{F}$ denotes the transverse Fourier transform. Thus the time-space representation of the impedance operator action is

$$(\mathcal{Y}^{-1}p_+)(\tilde{\boldsymbol{x}}, t) = \int_{\mathbb{R}^2}\int_0^t \frac{\delta'(t - t' - |\tilde{\boldsymbol{x}} - \tilde{\boldsymbol{x}}'|)}{2\pi|\tilde{\boldsymbol{x}} - \tilde{\boldsymbol{x}}'|}p_+(\tilde{\boldsymbol{x}}', t')\,\mathrm{d}t'\,\mathrm{d}x_1'\,\mathrm{d}x_2'\ , \tag{6.3}$$

for sufficiently smooth controls, p_+. Here, $\boldsymbol{x} \in \Gamma_{\mathrm{t}}$, $t \in [0, T]$.

In Section 6 and the Appendices, we use Fourier and Laplace transforms, to utilize their properties we consider the case that all fields, $p, \boldsymbol{v}$ and $q, \boldsymbol{u}$, to have temporal support contained in $[0, T]$. Consequently, the time-reversal operator is redefined as

$$(\mathcal{T}p_+)(\boldsymbol{x}, t) = p_+(\boldsymbol{x}, T - t)\ , \quad \boldsymbol{x} \in \Omega\ ,\ t \in [0, T]\ . \tag{6.4}$$

As the system is linear, and independent of starting time, the change of definition of $\mathcal{T}$, is only a matter of shifting the solution with respect to time.

$\mathcal{T}$ does not commute with an admittance $\mathcal{Y}$ of the form (6.1). Indeed observe that the adjoint $\mathcal{Y}^*$ of $\mathcal{Y}$ with respect to the standard L^2-inner product over time

and space at the boundary is

$$((\mathcal{Y}^*)^{-1}p_+)(\tilde{\boldsymbol{x}},t) = \int_{\mathbb{R}^2}\int_t^T \frac{\delta'(t'-t-|\tilde{\boldsymbol{x}}-\tilde{\boldsymbol{x}}'|)}{2\pi|\tilde{\boldsymbol{x}}-\tilde{\boldsymbol{x}}'|} p_+(\tilde{\boldsymbol{x}}',t')\,\mathrm{d}t'\,\mathrm{d}x_1'\,\mathrm{d}x_2' \,. \tag{6.5}$$

It follows that $\mathcal{Y}$ is not self-adjoint. By the variable substitution $\tau = T - t'$ we obtain

$$\begin{aligned}((\mathcal{Y}^*)^{-1}p_+)(\tilde{\boldsymbol{x}},t) &= \mathcal{T}\int_{\mathbb{R}^2}\int_0^t \frac{\delta'(t-\tau-|\tilde{\boldsymbol{x}}-\tilde{\boldsymbol{x}}'|)}{2\pi|\tilde{\boldsymbol{x}}-\tilde{\boldsymbol{x}}'|}(\mathcal{T}p_+)(\tilde{\boldsymbol{x}}',\tau)\,\mathrm{d}\tau\,\mathrm{d}x_1'\,\mathrm{d}x_2' \\ &= (\mathcal{T}\mathcal{Y}^{-1}\mathcal{T}p_+)(\tilde{\boldsymbol{x}},t)\,. \end{aligned} \tag{6.6}$$

6.2 Non-solvability of 'equal fields on the boundary'

In this section, we show that for the time reversal mirror configuration with the boundary condition (2.4) and admittance operator (6.3), the given algorithm does not have an optimal boundary control. We also derive an approximate boundary control, that agrees with the equation for optimal boundary control in the non-evanescent part of the measured field.

For the homogeneous half space, with transducers characteristics $\mathcal{Y}^{-1}$ as in (6.3), the boundary condition (2.4) is equivalent to a splitting of the field into an in- and outgoing field at the boundary [14–17]. Thus a transducer with the (6.3) characteristics is perfectly matched to the domain, and does not introduce any transducer mismatch reflections. Hence, as the medium is homogeneous, the response operator vanishes, *i.e.*, $\mathcal{R}p_+ = 0$.

If we consider the solvability of the requirement of equal fields on the boundary, with (6.6) the equations (3.11) reduce to

$$(\mathcal{Y}^{-1} + (\mathcal{Y}^*)^{-1})p_+ = 2(\mathcal{Y}^*)^{-1}\mathcal{T}q_-^{(0)}\,. \tag{6.7}$$

The operator $(\mathcal{Y}^{-1} + (\mathcal{Y}^*)^{-1})$ is not invertible everywhere on the range of $(\mathcal{Y}^*)^{-1}$. Thus the requirement of equal fields on the boundary is a too strong condition for this admittance. We analyze this situation; rewrite the least-square functional, $\mathcal{J}$, with the definitions of the boundary control and its observations, as

$$\mathcal{J} = E_0 + \int_0^T\int_{\Gamma_t}(\mathcal{Y}^{-1}p_+ - \mathcal{T}\mathcal{Y}^{-1}q_-^{(0)})(p_+ - \mathcal{T}q_-^{(0)})\,\mathrm{d}x_1\,\mathrm{d}x_2\,\mathrm{d}t\,, \tag{6.8}$$

where we have made the assumption that $q_+ = 0$. This assumption comes from the observation that q_+ does not have any measurable response at the boundary, and if a non-zero q_+ is applied at the boundary then $E_0(q_+ \neq 0) > E_0(q_+ = 0)$.

The least-squares functional $\mathcal{J}$ does not have any critical points for this choice of admittance. To see this, we denote the above integral over time and boundary by the inner product $\langle\cdot,\cdot\rangle_{\Gamma_t\times[0,T]}$, and we observe that the field is real-valued and that the operator $\mathcal{Y}^{-1}$ maps real-valued functions into real-valued functions. Upon

determining the variation with respect to p_+ we find the requirement for critical points to be

$$\langle \mathcal{D}\mathcal{J}, \delta p_+ \rangle_{\Gamma_t \times [0,T]} = \\ -2\,\mathrm{Re}\langle (\mathcal{Y}^{-1} + (\mathcal{Y}^*)^{-1}) p_+ - (\mathcal{T}\mathcal{Y}^{-1} + (\mathcal{Y}^*)^{-1}\mathcal{T}) q_-^{(0)}, \delta p_+ \rangle_{\Gamma_t \times [0,T]} = 0 \ , \quad (6.9)$$

for all $\delta p_+ \in \mathrm{L}^2$. Using the property (6.6) we find that (6.9) simplifies to

$$\langle (\mathcal{Y}^{-1} + (\mathcal{Y}^*)^{-1}) p_+, \delta p_+ \rangle_{\Gamma_t \times [0,T]} = \langle 2(\mathcal{Y}^*)^{-1}\mathcal{T} q_-^{(0)}, \delta p_+ \rangle_{\Gamma_t \times [0,T]} \ , \quad (6.10)$$

for all $\delta p_+ \in \mathrm{L}^2$. This equation is equivalent to (6.7) and to see its non-solvability for general $q_-^{(0)}$, we apply Parseval's formula to (6.10) and obtain

$$\mathrm{H}(\omega^2 - \tilde{\xi}^2) \frac{|\omega|}{\sqrt{\omega^2 - \tilde{\xi}^2}} p_+(\tilde{\boldsymbol{\xi}}, \omega) = \lim_{\eta \to 0^+} \frac{(\eta - \mathrm{i}\omega)}{\sqrt{(\eta - \mathrm{i}\omega)^2 + \tilde{\xi}^2}} \mathrm{e}^{-\mathrm{i}\omega T} q_-^{(0)}(\tilde{\xi}, -\omega) \ , \quad (6.11)$$

where $\mathrm{H}(\cdot)$ is the Heaviside step function. It is obvious that (6.11) does not have a solution for all $q_-^{(0)}$, in particular for $|\omega| < \tilde{\xi}$, since the left-hand side is zero whereas the right-hand side can be non-zero, depending on $q_-^{(0)}$. In the Fourier domain for the corresponding Green's function the frequency region $|\omega| < \tilde{\xi}$ is the non-propagating part of the field, hence we denote the part where $q_-^{(0)} \neq 0$ for $|\omega| < \tilde{\xi}$ as *the evanescent part* of $q_-^{(0)}$, *cf. e.g.*, [25]. Thus the equal fields on the boundary condition is not applicable in the time reversal mirror, and thus the algorithm does not yield an optimum for this case.

We conclude that for general $q_-^{(0)} \in \mathrm{L}^2$, the least-square functional, $\mathcal{J}$, does not have a critical point in terms of the field at the boundary. However, if $q_-^{(0)}$ does not have an evanescent part, then $\mathcal{J}$ has a critical point and the corresponding optimal control is

$$p_+ = \mathcal{T} q_-^{(0)}\big|_{|\omega| \geq \tilde{\xi}} \ . \quad (6.12)$$

6.3 Approximate boundary controls

As shown in Sec. 6.2 it is only possible to satisfy the equal fields on the boundary condition for the propagating part of the wave field. Hence, it is not clear how to choose the control in the non-propagating or evanescent part of the wave field. Here, we consider three different controls, labeled $p_+^{(1)}$, $p_+^{(2)}$, and $p_+^{(3)}$, that satisfy (6.10) in the propagating region. The first case, $p_+^{(1)}$ is the particle-velocity normalized control, *i.e.*, observation of the initial state $q_-^{(0)}$ is measured in particle-velocity normalization, time reversed and retransmitted, *viz.*,

$$p_+^{(1)} = \mathcal{T} q_-^{(0)} \ . \quad (6.13)$$

Case two: The corresponding pressure normalized boundary control $p_{+,\mathrm{N_p}}^{(2)}$ is to observe, $m_{(2)}$, the same initial state in pressure normalization, time reverse and retransmitted, *viz.*, $p_{+,\mathrm{N_p}}^{(2)} = \mathcal{T} m_{(2)}$, where the boundary condition and the observation

(2.4) and (2.6) are replaced with

$$\frac{p+\mathcal{Y}^{-1}v_3}{2}=p^{(2)}_{+,\mathrm{N_p}} \text{ and } \; m_{(2)}=\frac{p-\mathcal{Y}^{-1}v_3}{2}. \tag{6.14}$$

The boundary control $p^{(2)}_{+,\mathrm{N_p}}$ and observation $m_{(2)}$ can be expressed in pressure normalization[1] *viz.*,

$$p^{(2)}_{+}=\mathcal{Y}\mathcal{T}\mathcal{Y}^{-1}q^{(0)}_{-}. \tag{6.15}$$

Note that $\mathcal{Y}\mathcal{T}\mathcal{Y}^{-1}=\mathcal{T}\mathcal{Y}^{*}\mathcal{Y}^{-1}=\mathcal{Y}(\mathcal{Y}^{-1})^{*}\mathcal{T}$, by using (6.6).

The third case us the linear combination of the first two cases, *i.e.*,

$$p^{(3)}_{+}=p^{(1)}_{+}+p^{(2)}_{+}=(1+\mathcal{Y}(\mathcal{Y}^{-1})^{*})\mathcal{T}q^{(0)}_{-}. \tag{6.16}$$

Note from (6.11) that $p^{(3)}_{+}$ cuts the non-propagating part of the $q^{(0)}_{-}$. The results of case 3 is discussed in Section 6.7.

6.4 Control operators

In this section we derive the control operators for the respective normalization, for boundary data with temporal duration T, *i.e.*, an operator that takes the boundary control to the respective final states at $t=T$.

The control operator in particle velocity normalization is defined as:

$$\{p^{(1)}(\cdot,T),\boldsymbol{v}^{(1)}(\cdot,T)\}=\mathcal{W}_{\mathrm{v}}p^{(1)}_{+}\;. \tag{6.17}$$

To derive the explicit form of $\mathcal{W}_{\mathrm{v}}$, we solve the acoustic wave equation, (2.2) and (2.3) together with the transducer boundary condition (2.4) and quiescent initial conditions. We obtain (see Appendix A.1)

$$p^{(1)}(\boldsymbol{x},T)=\int_0^T\int_{\mathbb{R}^2}\frac{\delta(T-t'-|\boldsymbol{x}-\tilde{\boldsymbol{x}}'|)}{2\pi|\boldsymbol{x}-\tilde{\boldsymbol{x}}'|}\partial_{t'}\left(\mathrm{H}(t')p^{(1)}_{+}(\tilde{\boldsymbol{x}}',t')\right)\mathrm{d}x'_1\,\mathrm{d}x'_2\,\mathrm{d}t'\;, \tag{6.18}$$

and

$$\boldsymbol{v}^{(1)}(\boldsymbol{x},T)=-\nabla\int_0^T\int_{\mathbb{R}^2}\frac{\delta(T-t'-|\boldsymbol{x}-\tilde{\boldsymbol{x}}'|)}{2\pi|\boldsymbol{x}-\tilde{\boldsymbol{x}}'|}p^{(1)}_{+}(\tilde{\boldsymbol{x}}',t')\,\mathrm{d}x'_1\,\mathrm{d}x'_2\,\mathrm{d}t'\;. \tag{6.19}$$

The control operator in the pressure normalization, $\mathcal{W}_{\mathrm{p}}$, is obtained by solving the acoustic wave equation with transducer boundary condition (6.14), and quiescent initial conditions. We obtain (see Appendix C)

$$p^{(2)}(\boldsymbol{x},T)=-\partial_3\int_0^T\int_{\mathbb{R}^2}\frac{\delta(T-t'-|\boldsymbol{x}-\tilde{\boldsymbol{x}}'|)}{2\pi|\boldsymbol{x}-\tilde{\boldsymbol{x}}'|}p^{(2)}_{+,\mathrm{N_p}}(\tilde{\boldsymbol{x}}',t')\,\mathrm{d}x'_1\,\mathrm{d}x'_2\,\mathrm{d}t'\;, \tag{6.20}$$

[1]The equivalence of the field in the domain from the controls $p^{(2)}_{+}$ and $p^{(2)}_{+,\mathrm{N_p}}$ in the respective normalization is utilized to explicitly calculate the response of $p^{(2)}_{+}$, see Appendix C.

and

$$\boldsymbol{v}^{(2)}(\boldsymbol{x},T) = \nabla\partial_3 \int_0^T \int_{\mathbb{R}^2} \frac{\delta(T-t'-|\boldsymbol{x}-\tilde{\boldsymbol{x}}'|)}{2\pi|\boldsymbol{x}-\tilde{\boldsymbol{x}}'|} \int_0^{t'} p^{(2)}_{+,\mathrm{N_p}}(\tilde{\boldsymbol{x}}',t'')\,\mathrm{d}t''\,\mathrm{d}x'_1\,\mathrm{d}x'_2\,\mathrm{d}t' \,. \tag{6.21}$$

Thus we have an explicit expression for the control operator in both normalizations, expressed in terms of a common Green's function. Note that the form of the control operators have the typical retarded time dependence that is associated with hyperbolic systems.

6.5 The solution operator

In this section, we use the solution operator with initial conditions corresponding to a pressure pulse to derive the field at the boundary. We also construct the boundary controls for the two cases (6.13) and (6.15).

To construct the boundary controls, $p^{(1)}_+$, $p^{(2)}_{+,\mathrm{N_p}}$, corresponding to an initial pressure pulse, the time reversed output field component is needed as data. It is obtained by solving the acoustic equations (2.2) with the initial value $\{p_T, -\boldsymbol{v}_T\}$ at $t = 0$. The solution is [20]

$$\begin{pmatrix} q(\boldsymbol{x},t) \\ \boldsymbol{u}(\boldsymbol{x},t) \end{pmatrix} = \begin{pmatrix} \partial_t & -\nabla\cdot \\ -\nabla & I\partial_t \end{pmatrix} \int_{\mathbb{R}^3} \frac{\delta(t-|\boldsymbol{x}-\boldsymbol{x}'|)}{4\pi|\boldsymbol{x}-\boldsymbol{x}'|} \begin{pmatrix} p_T(\boldsymbol{x}') \\ -\boldsymbol{v}_T(\boldsymbol{x}') \end{pmatrix} \mathrm{d}x'_1\,\mathrm{d}x'_2\,\mathrm{d}x'_3 \,, \tag{6.22}$$

for an irrotational initial velocity, *i.e.*, $\nabla \times \boldsymbol{v}_T = 0$. Now, to generate the output field component at the boundary $\Gamma_{\mathrm{t}} = \{\boldsymbol{x} \in \mathbb{R}^3 : x_3 = 0\}$, we assume that supp p_T and supp $\boldsymbol{v}_T$ are bounded and contained in the half space $x_3 > 0$. Furthermore, we impose a transparent boundary condition at Γ_{t}, *i.e.*, no reflection at the boundary $x_3 = 0$. The boundary data in (6.13), (6.15) are measurement with perfectly matched receivers of the solution to (2.2) at the boundary, and does not change the solution (6.22).

To obtain an explicit representation of the field, we let the initial field be a pulse in the pressure, with source point $\tilde{\boldsymbol{x}} = 0$, $x_3 = z_0 > 0$, that is

$$p_T(\boldsymbol{x}) = \delta(\tilde{\boldsymbol{x}})\,\delta(x_3 - z_0) \quad \text{and} \quad \boldsymbol{v}_T = 0 \,. \tag{6.23}$$

The choice of pulse (6.23) substituted into (6.22) makes the field $\{q, \boldsymbol{u}\}$ into the components of the pressure Green's function. At the boundary its $\{q, u_3\}$-component becomes

$$\begin{aligned} \begin{pmatrix} q(\tilde{\boldsymbol{x}},0,t) \\ u_3(\tilde{\boldsymbol{x}},0,t) \end{pmatrix} &= \begin{pmatrix} \partial_t \\ -\partial_3 \end{pmatrix} \int_{\mathbb{R}^3} \frac{\delta(t-|\boldsymbol{x}-\boldsymbol{x}'|)}{4\pi|\boldsymbol{x}-\boldsymbol{x}'|}\,\delta(\tilde{\boldsymbol{x}}')\,\delta(x'_3 - z_0)\,\mathrm{d}x'_1\,\mathrm{d}x'_2\,\mathrm{d}x'_3\Big|_{x_3=0} \\ &= \begin{pmatrix} \partial_t \\ \partial_{z_0} \end{pmatrix} \frac{\delta(t-\sqrt{\tilde{x}^2+z_0^2})}{4\pi\sqrt{\tilde{x}^2+z_0^2}} \,. \end{aligned} \tag{6.24}$$

This field is measured by transducers yielding $q^{(0)}_-$, and $m_{(2)}$, respectively, see (2.6) and (6.14)

Here, the transducer is perfectly matched to the domain, equivalent to the transparent boundary condition, and measures the velocity normalized out-going component of the wave, *cf.* [18]. As the receiver and transducer characteristics are identical, the measured response $\{q_-^{(0)},\, m_{(2)}\}$ in the respective normalizations, case 1 and case 2, is (*cf.* (2.6) and (6.14))

$$q_-^{(0)}(\tilde{\boldsymbol{x}},t) = \frac{1}{2}\big((\mathcal{Y}q)(\tilde{\boldsymbol{x}},0,t) - u_3(\tilde{\boldsymbol{x}},0,t)\big)\ , \tag{6.25}$$

$$m_{(2)}(\tilde{\boldsymbol{x}},t) = \frac{1}{2}\left(q(\tilde{\boldsymbol{x}},0,t) - (\mathcal{Y}^{-1}u_3)(\tilde{\boldsymbol{x}},0,t)\right)\ . \tag{6.26}$$

Substituting the explicit field $\{q, u_3\}$ (*cf.* (6.24)) into (6.25) and (6.26) gives (see Appendix A.2 and Appendix C)

$$q_-^{(0)}(\tilde{\boldsymbol{x}},t) = -\partial_{z_0}\frac{\delta(t-\sqrt{\tilde{x}^2+z_0^2})}{4\pi\sqrt{\tilde{x}^2+z_0^2}}\ , \tag{6.27}$$

$$m_{(2)}(\tilde{\boldsymbol{x}},t) = \partial_t\frac{\delta(t-\sqrt{\tilde{x}^2+z_0^2})}{4\pi\sqrt{\tilde{x}^2+z_0^2}}\ . \tag{6.28}$$

The measurements, $\{q_-^{(0)},\ m_{(2)}\}$ of the field at the surface start at time $t=0$. We notice the expected delayed arrival in the measurement, because of the initial pulse is at depth $x_3 = z_0$. The 'measurement' ends at $t=T$ and, in general, the field at this time is non-zero. Hence, to describe the measured field, we have to introduce a step function that removes the field after $t=T$.

Now, time reversal in accordance with (6.4) of $q_-^{(0)}$ and $m_{(2)}$ are the controls that we search for,

$$p_+^{(1)}(\tilde{\boldsymbol{x}},t) = \mathrm{H}(t)q_-^{(0)}(\tilde{\boldsymbol{x}},T-t) = -\mathrm{H}(t)\partial_{z_0}\frac{\delta(T-t-\sqrt{\tilde{x}^2+z_0^2})}{4\pi\sqrt{\tilde{x}^2+z_0^2}}\ , \tag{6.29}$$

$$p_{+,\mathrm{N_p}}^{(2)}(\tilde{\boldsymbol{x}},t) = \mathrm{H}(t)m_{(2)}(\tilde{\boldsymbol{x}},T-t) = -\mathrm{H}(t)\partial_t\frac{\delta(T-t-\sqrt{\tilde{x}^2+z_0^2})}{4\pi\sqrt{\tilde{x}^2+z_0^2}}\ . \tag{6.30}$$

6.6 Retrofocused fields and their properties

Here, the explicit form of the retrofocused field in case 1 is used to analyze the long time limit of the retrofocused field. In the long time limit, case 1 retrofocuses the pressure perfectly, modulo a numerical factor, whereas the particle velocity shows a nonzero remainder, and is hence not perfectly retrofocused. We also give the explicit form of the pressure for case 2. We also show a number of graphs describing the degree of retrofocusing versus time duration of the measured data.

For the boundary control (6.29) we can explicitly obtain the final state as distributions, denoted by $\{p^{(1)}(\cdot,T), \boldsymbol{v}^{(1)}(\cdot,T)\}$, for any finite time T. Toward this end substitute the control $p_+^{(1)}$ of (6.29) into (6.18) and (6.19). Integration with respect

to time gives the response,

$$
\begin{aligned}
&p^{(1)}(\boldsymbol{x},T) = \\
&\quad -\partial_{z_0}\partial_t \int_{\mathbb{R}^2} \mathrm{H}(t-|\boldsymbol{x}-\tilde{\boldsymbol{x}}'|)\frac{\delta\big(T-t+|\boldsymbol{x}-\tilde{\boldsymbol{x}}'|-\sqrt{(\tilde{x}')^2+z_0^2}\big)}{8\pi^2|\boldsymbol{x}-\tilde{\boldsymbol{x}}'|\sqrt{(\tilde{x}')^2+z_0^2}}\,\mathrm{d}x_1'\,\mathrm{d}x_2'\bigg|_{t=T} \\
&\quad = \frac{-z_0}{4\pi^2 x_3\tilde{x}^2}\partial_3 \frac{\tilde{x}^2-x_3^2+z_0^2}{\Big([T^2-x_3^2-\big(\tilde{x}-\sqrt{T^2-z_0^2}\big)^2][\big(\tilde{x}+\sqrt{T^2-z_0^2}\big)^2+x_3^2-T^2]\Big)_+^{1/2}}
\end{aligned}
\tag{6.31}
$$

and

$$
\begin{aligned}
&\boldsymbol{v}^{(1)}(\boldsymbol{x},T) = \\
&\quad \nabla\partial_{z_0}\int_{\mathbb{R}^2} \mathrm{H}(t-|\boldsymbol{x}-\tilde{\boldsymbol{x}}'|)\frac{\delta(T-t+|\boldsymbol{x}-\tilde{\boldsymbol{x}}'|-\sqrt{(\tilde{x}')^2+z_0^2})}{8\pi^2|\boldsymbol{x}-\tilde{\boldsymbol{x}}'|\sqrt{(\tilde{x}')^2+z_0^2}}\,\mathrm{d}x_1'\,\mathrm{d}x_2'\bigg|_{t=T} \\
&\qquad = \nabla\Bigg[\frac{-z_0 T}{\pi^2\,(4\tilde{x}^2 z_0^2+(\tilde{x}^2+x_3^2-z_0^2)^2)} \\
&\qquad \frac{\tilde{x}^2-x_3^2+z_0^2}{\Big([T^2-x_3^2-\big(\tilde{x}-\sqrt{T^2-z_0^2}\big)^2][\big(\tilde{x}+\sqrt{T^2-z_0^2}\big)^2+x_3^2-T^2]\Big)_+^{1/2}}\Bigg]\,.
\end{aligned}
\tag{6.32}
$$

For details we refer to Appendix B.

The analogous derivation for case 2 yields, upon substituting the boundary control $p^{(2)}_{+,\mathrm{N_P}}$ of (6.30) into (6.20) and (6.21). Upon integration, see Appendix C, we find that

$$
\begin{aligned}
&p^{(2)}(\boldsymbol{x},T) = \frac{-1}{4\pi^2\tilde{x}^2}\partial_3 \\
&\qquad \frac{\tilde{x}^2-x_3^2+z_0^2}{\Big([T^2-x_3^2-\big(\tilde{x}-\sqrt{T^2-z_0^2}\big)^2][\big(\tilde{x}+\sqrt{T^2-z_0^2}\big)^2+x_3^2-T^2]\Big)_+^{1/2}}\,,
\end{aligned}
\tag{6.33}
$$

and

$$
\begin{aligned}
\boldsymbol{v}^{(2)}(\boldsymbol{x},T) = -\nabla\partial_3\int_{\mathbb{R}^2}\Bigg(&\mathrm{H}\Big(T-\sqrt{(\tilde{x}')^2+z_0^2}\Big)\frac{\delta(\sqrt{(\tilde{x}')^2+z_0^2}-|\boldsymbol{x}-\tilde{\boldsymbol{x}}'|)}{8\pi^2|\boldsymbol{x}-\tilde{\boldsymbol{x}}'|\sqrt{(\tilde{x}')^2+z_0^2}} \\
&-\delta\Big(T-\sqrt{(\tilde{x}')^2+z_0^2}\Big)\frac{\mathrm{H}(\sqrt{(\tilde{x}')^2+z_0^2}-|\boldsymbol{x}-\tilde{\boldsymbol{x}}'|)}{8\pi^2|\boldsymbol{x}-\tilde{\boldsymbol{x}}'|\sqrt{(\tilde{x}')^2+z_0^2}}\Bigg)\,\mathrm{d}x_1'\,\mathrm{d}x_2'\,.
\end{aligned}
\tag{6.34}
$$

The difference in pressure, between the pressure normalization and the particle velocity normalization, is the factor z_0/x_3. Furthermore observe that v_3 is zero on the x_3-axis for $x_3 \neq z_0$. The integration of the first term in (6.34) is analogous to the normal particle velocity normalization *cf.* (B.21).

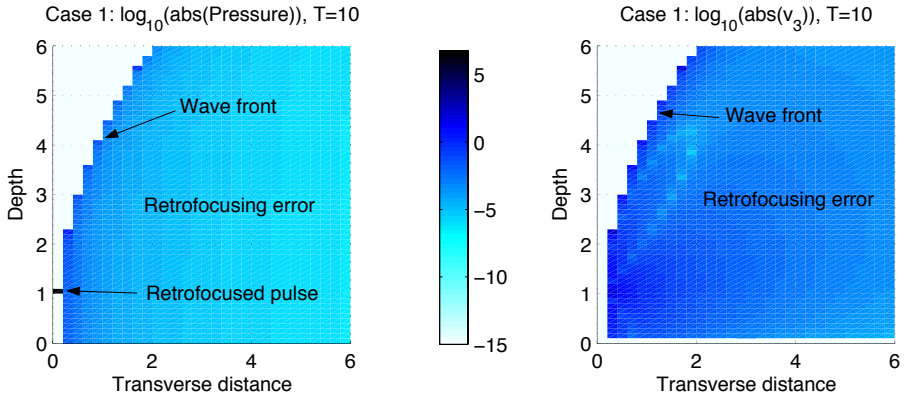

Figure 8: The retrofocused $p^{(1)}$ and $v_3^{(1)}$, for $T = 10$, with initial state a Dirac pulse at $z_0 = 1$, $\tilde{\boldsymbol{x}} = 0$, and its boundary control $p_+^{(1)}$. The pressure to high degree concentrated to $x_3 = 0$, $z_0 = 1$, with a small retrofocus error and the velocity have no corresponding concentration, *cf.* (6.35). The graphs show the boundary control, $p_+^{(1)}$ is imposed at depth $x_3 = 0$, and has a support for $x_3 = 0$ and $\tilde{x} \leq \sqrt{T^2 - z_0^2}$. In the graph notice the out-going wave-front with radius $T = 10$ with center located at all $\tilde{\boldsymbol{x}}$ such that $|\tilde{\boldsymbol{x}}| = \sqrt{T^2 - z_0^2}$, here at $\{\tilde{x}, x_3\} = \{\sqrt{99}, 0\}$, due to the finite time cutoff of the measurement. Recall that the graphs are distributions, hence it is smoothed around the wave-front set.

The first observation on the above final state is that $p^{(1)}, p^{(2)}$ and $v_3^{(1)}$ depend only on $\tilde{x}$ and not $\tilde{\boldsymbol{x}}$, *i.e.*, they are independent of polar angle — the angle between x_1 and x_2. The denominator $(...)_+^{1/2}$ describes wave fronts induced from the non-zero field at the end of a finite measurement time. These wave fronts are centered on the circle $x_3 = 0$, $\{\tilde{\boldsymbol{x}} : \tilde{x} = \sqrt{T^2 - z_0^2}\}$. The cut off in $(...)_+^{1/2}$, with the polar angle symmetry, makes the resulting field to have a domain that resembles a donut, cut horizontally just below the middle, in shape. A cross section of the field is shown in Figure 8 for $T = 10$, *i.e.*, the excitation time equals ten times the time it takes for the initial pulse reach the surface.

With the retrofocusing of this pulse, note that for an expansion as $T \to \infty$,

$$p^{(1)} = \frac{z_0}{4\pi^2}\Big(T^{-1}\tilde{x}^{-3} + (2T)^{-3}\big(\tilde{x}^{-1} + 2\tilde{x}^{-3}(x_3^2 + z_0^2) + 3\tilde{x}^{-5}(x_3^2 - z_0^2)\big)\Big) + \mathrm{O}(T^{-5}) \,,$$

and

$$v_3^{(1)} = \frac{x_3 z_0\big((x_3^2 - z_0^2)^2 - 3\tilde{x}^4 - 2\tilde{x}^2(x_3^2 + z_0^2)\big)}{\pi^2\tilde{x}\big(\tilde{x}^4 + (x_3^2 - z_0^2)^2 + 2\tilde{x}^2(x_3^2 + z_0^2)\big)^2} + \mathrm{O}(T^{-2}) \,, \tag{6.35}$$

together with

$$\begin{pmatrix} v_1^{(1)} \\ v_2^{(1)} \end{pmatrix} = \left(\frac{z_0(3\tilde{x}^2 + 4z_0^2)}{2\pi^2\tilde{x}^2(\tilde{x}^2 + 4z_0^2)}\begin{pmatrix}\cos\theta \\ \sin\theta\end{pmatrix} + \mathrm{O}\big((x_3 - z_0)^2\big)\right) + \mathrm{O}(T^{-2}) \,, \tag{6.36}$$

where θ is the polar angle. Furthermore, at the axis $\tilde{x} = 0$ the retrofocused field is supported only for $x_3 = z_0$. In Figure 9 we plot the pressure away from the singular

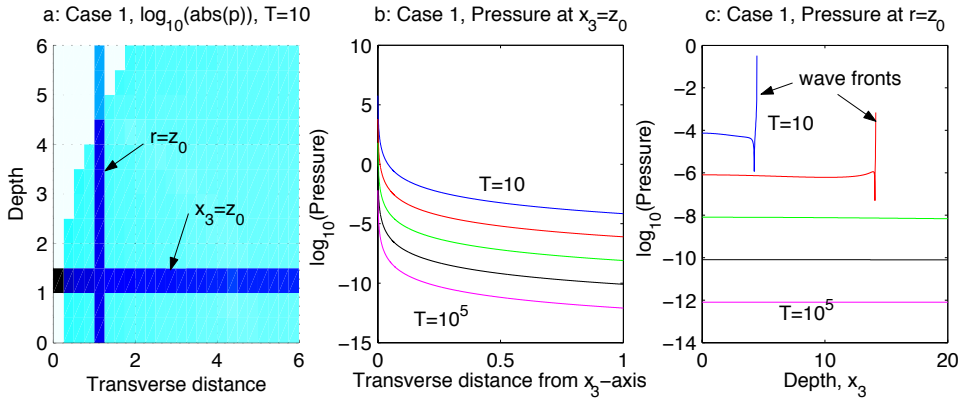

Figure 9: Plots of the pressure, for different excitation times T. In graph b,c each lower line corresponds to the T, values 10, 10^2, 10^3, 10^4, 10^5. a: The black lines indicates where the values in graph b and c are taken. b: At $x_3 = z_0$ we see the damping to the Dirac pulse, for the area around the singular point. c: At $r := |\tilde{\boldsymbol{x}}| = z_0$ we see that the fields damps as T increase, the ending of the two top lines are due to that we have reached the wave front, *cf.* Figure 9a.

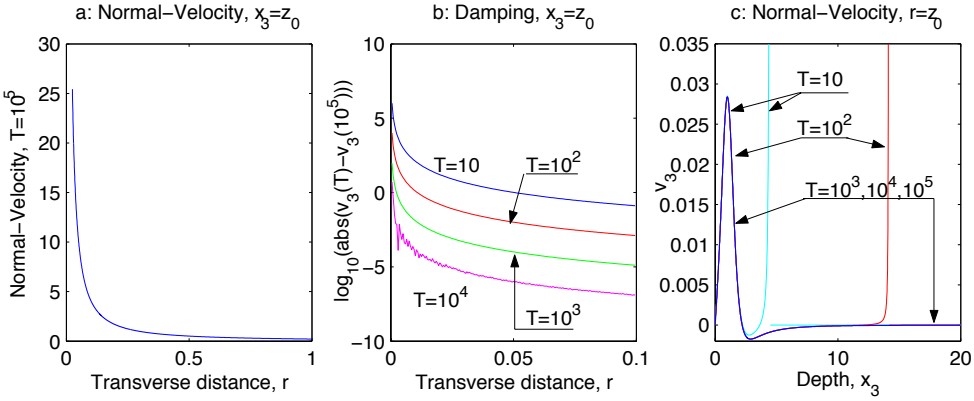

Figure 10: Plots of $v_3^{(1)}$ for a source at depth $z_0 = 1$ and its boundary control $p_+^{(1)}$. In a: The 'remaining' field as T becomes large *cf.* (6.35). b: Plots $\log_{10}(|v_3^{(1)}(T) - v_3^{(1)}(t = 10^5)|)$ for T =10, 10^2, 10^3, 10^4, along $x_3 = z_0$. In the lowest line the unevenness is due to numerical inaccuracies. c: Shows $v_3^{(1)}$ along $r := |\tilde{\boldsymbol{x}}| = z_0$ for times $T = 10 - -10^5$. All lines start along the same 'remaining' velocity at $x_3 = 0$. The first to deviate is $v_3^{(1)}(T = 10)$, that encounters its wave front at $x_3 \approx 4$, *cf.* Figure 8b, the next to go off to infinity, is $T = 10^2$ that encounters its wave front at $x_3 \approx 15$.

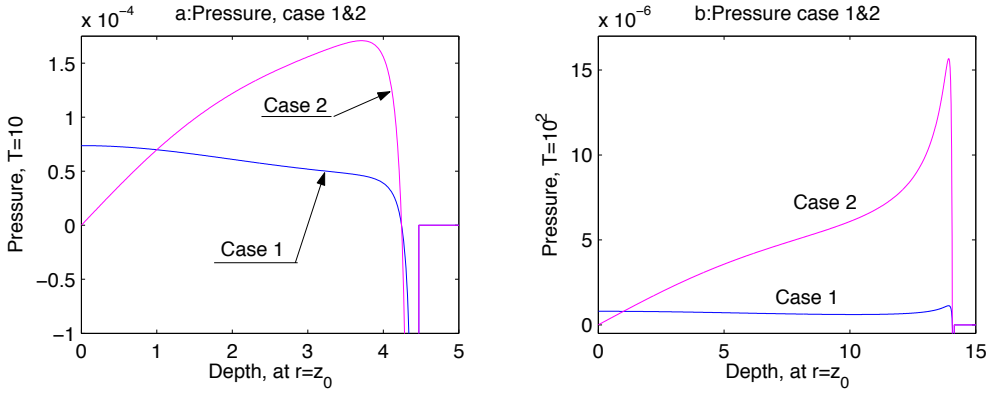

Figure 11: Comparison between case 1 and 2. The plots are along $r := |\tilde{\boldsymbol{x}}| = z_0$ a: The pressure, for $T = 10$. The wave front appears at $r \approx 4$. b: The same plot as in Figure 11a but with $T = 10^2$.

point for different excitation times T. It is apparent that the field is rapidly damped with respect to T and $\tilde{x}$. The analogous plots for v_3 are shown in Figure 10, where it is apparent that v_3 approaches its remaining, non-zero distribution rapidly.

In the limit $T \to \infty$ we obtain for the pressure, (Appendix D)

$$\lim_{T\to\infty} \int p^{(1)}(\tilde{\boldsymbol{x}}, x_3, T)\phi(\tilde{x}, x_3)\,\mathrm{d}x_1\,\mathrm{d}x_2\,\mathrm{d}x_3 = \frac{1}{2}\phi(0, z_0)\ , \tag{6.37}$$

for a compactly supported test function ϕ. This result agrees with the result presented in [14], obtained by an argument that utilized symmetries of the cavity case.

Thus we obtain a perfect retrofocusing in the pressure component, modulo an amplitude factor of 2, even in the presence of an evanescent component in the control.

6.7 Influence of evanescent part of the boundary control

Here, we discuss the influence of the evanescent part of the boundary control on the resulting fields.

As we noted in 6.3, the two given boundary controls differ only in the evanescent part, and thus by comparing the responding fields of respective case, we compare controls that only differ in the evanescent region. As we only derived the pressure component of the pressure normalized fields explicitly, let us study the difference in pressure. The pressure field differs only by a factor x_3/z_0, hence the difference is independent of time. To understand the difference between the retrofocused fields we plot the pressure for $\tilde{x} = z_0$, see Figure 11.

For case 1, we proved that as $T \to \infty$ the pressure concentrate at the source point $x_3 = z_0$, $\tilde{x} = 0$, the appearance of the factor x_3/z_0 for case 2 does not change the conclusion for $T \to \infty$, as $x_3/z_0 = 1$ at the source point. From the plots in Figure 11 we notice the apparent difference between the two cases, but upon observation of the amplitudes involved we conclude that for sufficiently large T, the evanescent part of the control has a negligible influence. As both cases of controls have a pressure

component that converge to a pulse, so must their sum, the response to $p_+^{(3)}$, as the acoustic wave equation is linear.

But, as we have already shown that the sum of the two controls does not have an evanescent part, and still it converges to the pressure Dirac pulse, the influence of the evanescent part, in the long time limit, is small on the pressure component of the final state. As the initial pressure is a Dirac pulse, this implies that for any initial state with quiescent velocity and non-zero pressure distribution, the evanescent part of the field has a marginal effect for sufficient long excitation times.

7 Discussion

The use of time-reversal in experiments and theory, both for linear acoustics and electro-magnetics, has increased rapidly the last years. Here, we develop an iterative time-reversal algorithm for the purpose of retrofocusing that differs from the iterative time-reversal algorithms described by M. Fink *et al.*, [2, 5, 9–13, 26] and M. Cheney *et al.*, [6, 7]. The algorithms are identical in the first step where they reduce to classical time reversal. The present algorithm retrofocuses the wave field towards the controllable part of its originating distribution, *i.e.*, it uses the transducers in an optimal way to recreate the original initial wave field. This is achieved by the construction of identical fields at the transducers in the original and retrofocused states. In contrast to this, the iterative time-reversal algorithm described in Refs 6, 7, 10 retransmit the wave field such that the reflection is maximized. This produces a focusing on the largest scatterer and largest eigenfunction in [10] and [6, 7], respectively.

The iterative time-reversal algorithm is especially useful in strongly multiple scattering cases such as the cavity described in Section 5. For this type of geometries, a few iterations improve the retrofocusing as illustrated by the numerical examples. For the time-reversal mirror examined in this paper, the iterative time-reversal algorithm reduce to the classical time reversal since the homogeneous half space is non-reflecting. But also in this case the boundary control analysis shows that the iterative time-reversal algorithm is optimally retrofocusing, in the least-square sense, when the evanescent part of the measured wave field is negligible.

In the half-space geometry, both a direct time reversal of the recorded wave field and a weighed time reversal is considered. The two controls are differ only in the evanescent part of the wave field. The analytic representation of the pressure field is given for the two controls when the initial field is a pressure Dirac pulse. As expected, the retrofocusing is not perfect, *i.e.*, only the controllable part of the wave field is retrieved. In this case the controllable part is essentially half of the wave field since only the up-going part [18] of the original pressure pulse reach the surface and is retransmitted as a down going wave field. The retrofocused field concentrate around the initial pulse point, and as the excitation time approach infinity, the pressure pulse retrofocus to half the initial pulse. However, the velocity component does not vanish in the large time limit.

Acknowledgments

This work is partially funded by a grant from the Swedish Research Council for Engineering Sciences and, for the first author, the Wenner-Gren Foundation, their support is gratefully acknowledged.

Appendix A Calculations on the half-space

A.1 Derivation of the control operator

Here, we give the explicit derivations to obtain the control operator for the particle velocity normalization.

To derive the control operator for the homogeneous half-space, we solve the system of equations

$$\begin{cases} \partial_t p + \nabla \cdot \boldsymbol{v} = 0 \,, & \boldsymbol{x} \in \Omega \,, & t \in (0, T] \,, \\ \partial_t \boldsymbol{v} + \nabla p = 0 \,, & \boldsymbol{x} \in \Omega \,, & t \in (0, T] \,, \\ p = 0 \,, \ \boldsymbol{v} = 0 \,, & \boldsymbol{x} \in \Omega \,, & t = 0 \,, \\ \frac{1}{2}(\mathcal{Y} p + v_3) = p_+^{(1)} \,, & \boldsymbol{x} \in \partial\Omega \,, & t \in [0, T] \,, \end{cases} \tag{A.1}$$

where the boundary condition is in the particle velocity normalization.

We Laplace transform the field in time, and with the use of $p(\boldsymbol{x}, 0) = 0$ and $\boldsymbol{v}(\boldsymbol{x}, 0) = 0$, together with the enforced causality, the resulting field are analytic for $\operatorname{Re} s \geq 0$. Furthermore, the correspondence $\partial_t \to s$ holds. We Fourier transform the transverse coordinates, $\tilde{\boldsymbol{x}} \to \tilde{\boldsymbol{\xi}}$, and upon eliminating the transverse particle velocities we obtain the 'two-way' equation for linear acoustic waves

$$\begin{cases} (\partial_3 + \boldsymbol{a}) f(\tilde{\boldsymbol{\xi}}, x_3, s) = 0 \,, & x_3 > 0 \,, \\ \boldsymbol{y} p + v_3 = p_+^{(1)}(\tilde{\boldsymbol{\xi}}, s) \,, & x_3 = 0 \,, \\ s \boldsymbol{v}_\perp(\tilde{\boldsymbol{\xi}}, x_3, s) + \mathrm{i}\tilde{\boldsymbol{\xi}} p(\tilde{\boldsymbol{\xi}}, x_3, s) = 0 \,, & x_3 > 0 \,, \end{cases} \tag{A.2}$$

$f = (p, v_3)$ and where the admittance operator symbol, $\boldsymbol{y}$, is defined in (6.1). Here, the acoustic system's matrix, $\boldsymbol{a}$, has the form

$$\boldsymbol{a} = \begin{pmatrix} 0 & s \\ s + s^{-1}\tilde{\xi}^2 & 0 \end{pmatrix} \,. \tag{A.3}$$

The formal solution to (A.2) is derived through wave splitting, see *e.g.*, [14, 15, 17], also notice the freedom of 'normalization', pointed out in [16–18], the normalization is arbitrary and related to the transducers characteristics, here we have chosen boundary condition in the particle velocity normalization, *i.e.*, $p_+^{(1)}$ is of 'dimension' particle velocity. The formal solution to (A.2) is

$$\begin{cases} f(\tilde{\boldsymbol{\xi}}, x_3, s) & = \mathrm{e}^{-x_3\sqrt{s^2+\tilde{\xi}^2}} \boldsymbol{\eta}^+ p_+^{(1)}(\tilde{\boldsymbol{\xi}}, s) \,, \\ \boldsymbol{v}_\perp(\tilde{\boldsymbol{\xi}}, x_3, s) & = -\frac{\mathrm{i}\tilde{\boldsymbol{\xi}}}{s} \mathrm{e}^{-x_3\sqrt{s^2+\tilde{\xi}^2}} \big(\boldsymbol{\eta}^+ p_+^{(1)}(\tilde{\boldsymbol{\xi}}, s)\big)_1 \,, \end{cases} \tag{A.4}$$

where $\boldsymbol{\eta}^+$, $(\boldsymbol{\eta}^-)$ is the eigenvector corresponding to the positive (negative) eigenvalue, $\pm\sqrt{s^2+\tilde{\xi}^2}$ of $\boldsymbol{a}$, and has the form, in particle velocity normalization

$$\boldsymbol{\eta}^{\pm} = \begin{pmatrix} \frac{s}{\sqrt{s^2+\tilde{\xi}^2}} \\ \pm 1 \end{pmatrix} . \tag{A.5}$$

With the above reformulations, the symbol of the control operator, $\mathcal{W}_{\mathrm{v}}$, becomes

$$\boldsymbol{w}^+ = \mathrm{e}^{-x_3\sqrt{s^2+\tilde{\xi}^2}} \begin{pmatrix} \frac{s}{\sqrt{s^2+\tilde{\xi}^2}} \\ -\frac{\mathrm{i}\tilde{\boldsymbol{\xi}}}{\sqrt{s^2+\tilde{\xi}^2}} \\ 1 \end{pmatrix} . \tag{A.6}$$

To transform this operator back into space and time, we observe the identity

$$\mathcal{F}^{-1}\frac{\mathrm{e}^{-x_3\sqrt{s^2+\tilde{\xi}^2}}}{\sqrt{s^2+\tilde{\xi}^2}} = \int_0^\infty \frac{\tilde{\xi}\,\mathrm{J}_0(\tilde{\xi}\tilde{x})\mathrm{e}^{-x_3\sqrt{s^2+\tilde{\xi}^2}}}{2\pi\sqrt{s^2+\tilde{\xi}^2}}\,\mathrm{d}\tilde{\xi} = \frac{\mathrm{e}^{-s|\boldsymbol{x}|}}{2\pi|\boldsymbol{x}|} , \tag{A.7}$$

by using Purdnikov, Brychkov and Marichev's volume 2, relation 2.12.10.10 [27]. Thus

$$\mathcal{L}^{-1}\mathcal{F}^{-1}\frac{\mathrm{e}^{-x_3\sqrt{s^2+\tilde{\xi}^2}}}{\sqrt{s^2+\tilde{\xi}^2}} = \frac{\delta(t-|\boldsymbol{x}|)}{2\pi|\boldsymbol{x}|} , \tag{A.8}$$

and as the inverse transform of this integral kernel is known, we express the symbol of the control operator, $\boldsymbol{w}^+$, in terms of the above kernel as

$$\begin{pmatrix} p \\ \tilde{\boldsymbol{v}} \\ v_3 \end{pmatrix} = (\boldsymbol{w}^+ p_+^{(1)})(\tilde{\boldsymbol{\xi}}, x_3, s) = \begin{pmatrix} s \\ -\mathrm{i}\tilde{\boldsymbol{\xi}} \\ -\partial_3 \end{pmatrix} \frac{\mathrm{e}^{-x_3\sqrt{s^2+\tilde{\xi}^2}}}{\sqrt{s^2+\tilde{\xi}^2}} p_+^{(1)}(\tilde{\boldsymbol{\xi}}, s) , \tag{A.9}$$

where $\tilde{\boldsymbol{v}} = \{v_1, v_2\}$. Using (A.8) on (A.9) we find that

$$p(\boldsymbol{x}, T) = \int_0^T \int_{\mathbb{R}^2} \frac{\delta(T-t'-|\boldsymbol{x}-\tilde{\boldsymbol{x}}'|)}{2\pi|\boldsymbol{x}-\tilde{\boldsymbol{x}}'|} \partial_{t'}\left(\mathrm{H}(t') p_+^{(1)}(\tilde{\boldsymbol{x}}', t')\right) \mathrm{d}x_1' \,\mathrm{d}x_2' \,\mathrm{d}t' , \tag{A.10}$$

and

$$\boldsymbol{v}(\boldsymbol{x}, T) = -\nabla \int_0^T \int_{\mathbb{R}^2} \frac{\delta(T-t'-|\boldsymbol{x}-\tilde{\boldsymbol{x}}'|)}{2\pi|\boldsymbol{x}-\tilde{\boldsymbol{x}}'|} p_+^{(1)}(\tilde{\boldsymbol{x}}', t') \,\mathrm{d}x_1' \,\mathrm{d}x_2' \,\mathrm{d}t' . \tag{A.11}$$

Thus we have an explicit expression for the control operator, when the boundary condition is in the particle velocity normalization. The control operator gives the field inside the domain, once the control at the boundary is known.

A.2 The measured data

In this section a calculation to obtain the explicit form of the measured field at the boundary for case 1 is presented.

From (6.25) we have that the measured data has the form

$$q_-^{(0)}(\tilde{\boldsymbol{x}},t) = \frac{1}{2}\big((\mathcal{Y}q)(\tilde{\boldsymbol{x}},0,t) - u_3(\tilde{\boldsymbol{x}},0,t)\big)\ , \tag{A.12}$$

In the Laplace–Fourier domain the equivalent field has the representation

$$q_-^{(0)}(\tilde{\boldsymbol{\xi}},s) = \frac{1}{2}\left(s^{-1}q(\tilde{\boldsymbol{\xi}},0,s)\sqrt{s^2+\tilde{\xi}^2} - u_3(\tilde{\boldsymbol{\xi}},0,s)\right)\ . \tag{A.13}$$

With the relation (A.8) we Laplace–Fourier transform the field $\{q(\tilde{\boldsymbol{x}},0,t), u_3(\tilde{\boldsymbol{x}},0,t)\}$, at the boundary, *cf.* (6.24). Substituting the result into (A.13) gives

$$\begin{pmatrix} q(\tilde{\boldsymbol{\xi}},0,s) \\ u_3(\tilde{\boldsymbol{\xi}},0,s)\end{pmatrix} = \frac{1}{2}\mathrm{e}^{-z_0\sqrt{s^2+\tilde{\xi}^2}}\boldsymbol{\eta}^-(\tilde{\boldsymbol{\xi}},s) \quad\Rightarrow\quad q_-^{(0)}(\tilde{\boldsymbol{\xi}},s) = \frac{1}{2}\mathrm{e}^{-z_0\sqrt{s^2+\tilde{\xi}^2}}\ , \tag{A.14}$$

where $\boldsymbol{\eta}^-$ is an eigenvector of $\boldsymbol{a}$ in the particle velocity normalization, see (A.5). In the time-space domain, using (A.8), we find that

$$q_-^{(0)}(\tilde{\boldsymbol{x}},t) = -\partial_{z_0}\frac{\delta(t-\sqrt{\tilde{x}^2+z_0^2})}{4\pi\sqrt{\tilde{x}^2+z_0^2}}\ . \tag{A.15}$$

Appendix B The field in the domain for the control $p_+^{(1)}$

Given the control $p_+^{(1)}$ in (6.29), we substitute it into (6.18) and (6.19). Below we explicitly calculate the two resulting distributions.

B.1 The pressure component

In this section we give a detailed derivation of the pressure distribution for the case 1.

Let us introduce the help quantities,

$$R_1 = \sqrt{(\tilde{x}')^2+z_0^2}\ , \quad R_2 = \sqrt{|\tilde{\boldsymbol{x}}-\tilde{\boldsymbol{x}}'|^2+x_3^2}\ , \ \text{ and } \ \tau = T-t\ , \tag{B.1}$$

with this notation the pressure, $p^{(1)}$, is represented as

$$p^{(1)}(\boldsymbol{x},t) = -\partial_{z_0}\partial_t\int_{\mathbb{R}^2}\mathrm{H}(t-R_2)\frac{\delta\big(\tau+(R_2-R_1)\big)}{8\pi^2R_1R_2}\,\mathrm{d}x_1'\,\mathrm{d}x_2' = \\ \partial_{z_0}x_3^{-1}\partial_3\int_{\mathbb{R}^2}\mathrm{H}(t-R_2)\frac{\delta\big(\tau+(R_2-R_1)\big)}{8\pi^2R_1}\,\mathrm{d}x_1'\,\mathrm{d}x_2'\ . \tag{B.2}$$

The delta Dirac traces out a curve for $\tilde{\boldsymbol{x}}'$, to find the curve consider the $\tilde{\boldsymbol{x}}'$ such that $R_1 - R_2 - \tau = 0$

$$\begin{aligned} R_1^2 = (\tau + R_2)^2 &= \tau^2 + R_2^2 + 2\tau R_2 \Leftrightarrow \\ -\tau\sqrt{x_3^2 + |\tilde{\boldsymbol{x}} - \tilde{\boldsymbol{x}}'|^2} &= (\tilde{x}^2 + x_3^2 - z_0^2 + \tau^2)/2 - \tilde{\boldsymbol{x}} \cdot \tilde{\boldsymbol{x}}' \Leftrightarrow \\ \tau^2(x_3^2 + \tilde{x}^2 + (\tilde{x}')^2 - 2\tilde{\boldsymbol{x}} \cdot \tilde{\boldsymbol{x}}') &= \left((\tilde{x}^2 + x_3^2 - z_0^2 + \tau^2)/2 - \tilde{\boldsymbol{x}} \cdot \tilde{\boldsymbol{x}}'\right)^2 \Leftrightarrow \\ \tau^2(x_3^2 + \tilde{x}^2) - A^2/4 &= -\tau^2(\tilde{x}')^2 + (\tilde{\boldsymbol{x}} \cdot \tilde{\boldsymbol{x}}')^2 - A(\tilde{\boldsymbol{x}} \cdot \tilde{\boldsymbol{x}}') \end{aligned} \tag{B.3}$$

hence a conical surface. Here,

$$A = \tilde{x}^2 + x_3^2 - z_0^2 + \tau^2 \ . \tag{B.4}$$

We observe the freedom of choice in the coordinates $\tilde{\boldsymbol{x}}'$, hence we choose the particular coordinate system for $\tilde{\boldsymbol{x}}'$, such that $\tilde{\boldsymbol{x}} = (\tilde{x}, 0)$, this is equivalent to rotate the coordinate system of $\tilde{\boldsymbol{x}}'$. The compatibly condition imposed on the solution associated with the square roots is

$$-\operatorname{sgn}(\tau) = \operatorname{sgn}(\tilde{x}^2 + x_3^2 - z_0^2 + \tau^2 - 2\tilde{x}x_1') \ , \tag{B.5}$$

as is observed from the second line of (B.3). Now we rewrite (B.3) into a more standard form for conical surfaces

$$c = (\tilde{x}^2 - \tau^2)(x_1' - x_1^0)^2 - \tau^2(x_2')^2 \ , \tag{B.6}$$

hence the set of $\{x_1', x_2'\}$, that fulfills (B.6), traces out a curve in space. In this case

$$x_1^0 = \tilde{x}\frac{A/2 - \tau^2}{\tilde{x}^2 - \tau^2} \quad \text{and} \quad c = \tau^2(x_3^2 + \tilde{x}^2) - A^2/4 + (\tilde{x}^2 - \tau^2)(x_1^0)^2 \ . \tag{B.7}$$

We notice that if $\tilde{x} > \tau$, the curved traced out is an hyperbola, when $\tilde{x} < \tau$, an ellipse and when $\tilde{x} = \tau$, it is a line parallel to x_1'-axis.

In evaluating the integral (B.2) we consider only the limiting case when $t = T$ *i.e.*, $\tau = 0$. Thus the integral reduces to

$$p^{(1)}(\boldsymbol{x}, T) = \frac{1}{x_3}\partial_{z_0}\partial_3 \int_{\mathbb{R}^2} \mathrm{H}(T - R_2)\frac{\delta(R_2 - R_1)}{8\pi^2 R_1}\,\mathrm{d}x_1'\,\mathrm{d}x_2' \ . \tag{B.8}$$

We find that

$$x_1^0 = A/(2\tilde{x}) = \frac{\tilde{x}}{2}\left(1 + \frac{x_3^2 - z_0^2}{\tilde{x}^2}\right) \ , \quad c = 0 \ , \quad A = \tilde{x}^2 + x_3^2 - z_0^2 \ , \tag{B.9}$$

and the conical curve (B.6) collapses into the line

$$x_1' = x_1^0 \quad \Rightarrow \quad x_1 = \frac{\tilde{x}}{2}\left(1 + \frac{x_3^2 - z_0^2}{2\tilde{x}^2}\right) \ . \tag{B.10}$$

This line fulfills the compatibly condition (B.5), hence it is a solution.

To evaluate the integral we introduce a change of coordinates, let the new coordinates be: $\Psi = R_1 - R_2$ and the arc length, s, along the line (B.10). The integral in those coordinates collapses into an integral with integrand

$$(R_2|\nabla\Psi|)^{-1}\,\mathrm{d}s = \tilde{x}^{-1}\,\mathrm{d}x_2' \,, \tag{B.11}$$

to see this, first note that

$$\mathrm{d}s = \sqrt{1 + \Big(\frac{\partial x_1'}{\partial x_2'}\Big)^2}\,\mathrm{d}x_2' = \mathrm{d}x_2' \,, \tag{B.12}$$

and

$$(R_1R_2)^2|\nabla'(R_1 - R_2)|^2_{\Psi=0} = |(R_2 - R_1)\tilde{\boldsymbol{x}}' + R_1\tilde{\boldsymbol{x}}|^2_{\Psi=0} = R_1^2\tilde{x}^2\big|_{\Psi=0} \,, \tag{B.13}$$

where we have used $R_1 = R_2$, or equivalently $x_1' = x_1^0$. Hence, the pressure integral becomes

$$p^{(1)}(\boldsymbol{x}, T) = \frac{1}{8\pi^2\tilde{x}x_3}\partial_{z_0}\partial_3 \int_{\mathbb{R}} \mathrm{H}(T - R_1)|_{R_1=R_2}\,\mathrm{d}x_2' \,, \tag{B.14}$$

i.e., the length of the line, $x_1' = x_1^0$, inside the circle described by $\mathrm{H}(T - R_1)$. The height, x_2', where $x_1' = x_1^0$ crosses the circle is

$$T^2 = z_0^2 + (x_1')^2 + (x_2')^2\big|_{x_1'=x_1^0} = z_0^2 + (x_1^0)^2 + (x_2')^2 \quad \Rightarrow$$
$$x_2' = \pm\sqrt{T^2 - z_0^2 - (x_1^0)^2}, \tag{B.15}$$

hence

$$p^{(1)}(\boldsymbol{x}, T) = \frac{1}{4\pi^2\tilde{x}x_3}\partial_{z_0}\partial_3\left(\sqrt{T^2 - (z_0^2 + (x_1^0)^2)}\mathrm{H}(T - \sqrt{z_0^2 + (x_1^0)^2})\right) \,. \tag{B.16}$$

We now let the derivative with respect to the parameter z_0 act on the distribution. We first observe that

$$\partial_{z_0}\sqrt{T^2 - (z_0^2 + (x_1^0)^2)} = \frac{-z_0(x - x_1^0)}{\tilde{x}\sqrt{T^2 - z_0^2 - (x_1^0)^2}} \,, \tag{B.17}$$

so that

$$p^{(1)}(\boldsymbol{x}, T) = \frac{-z_0}{4\pi^2 x_3\tilde{x}^2}\partial_3\frac{\tilde{x} - x_1^0}{(T^2 - z_0^2 - (x_1^0)^2)_+^{1/2}} =$$
$$\frac{-z_0}{4\pi^2 x_3\tilde{x}^2}\partial_3\frac{\tilde{x}^2 - x_3^2 + z_0^2}{(4\tilde{x}^2(T^2 - z_0^2) - A^2)_+^{1/2}} \,. \tag{B.18}$$

We rewrite the denominator in the form

$$\left(\Big[T^2 - x_3^2 - \Big(\tilde{x} - \sqrt{T^2 - z_0^2}\Big)^2\Big]\Big[\Big(\tilde{x} + \sqrt{T^2 - z_0^2}\Big)^2 + x_3^2 - T^2\Big]\right)_+^{1/2} \,, \tag{B.19}$$

where the plus sign indicates that we consider it as generalized function, and the value within the outer parentheses must be positive. With (B.18) and (B.19), we have obtained the pressure inside the domain corresponding to the control $p_+^{(1)}$. It is a distribution, and is considered as acting on smooth test functions.

B.2 The velocity component

With the same notation as in the previous section, we write the particle velocity inside the domain, for the boundary control $p_+^{(1)}$, in the limit $t = T$ as

$$\boldsymbol{v}^{(1)}(\boldsymbol{x}, T) = \nabla\partial_{z_0} \int_{\mathbb{R}^2} \mathrm{H}(T - R_2) \frac{\delta(R_2 - R_1)}{8\pi^2 R_1 R_2} \,\mathrm{d}x_1' \,\mathrm{d}x_2' \,. \tag{B.20}$$

With the change to the arc-length coordinates, we have, (*cf.* (B.11))

$$\boldsymbol{v}^{(1)}(\boldsymbol{x}, T) = \nabla \frac{1}{8\pi^2 \tilde{x}} \partial_{z_0} \int_{\mathbb{R}} \frac{\mathrm{H}(T - R_2)}{R_1}\bigg|_{R_1 = R_2} \mathrm{d}x_2' \,. \tag{B.21}$$

Analogous to the derivation leading up to (B.10), the condition $R_1 = R_2$ is equivalent to $x_1' = x_1^0$, hence

$$R_1|_{x_1' = x_1^0} = \big((x_1^0)^2 + z_0^2 + (x_2')^2\big)^{1/2} \,. \tag{B.22}$$

The integral is straight forward, once we notice that the step function imposes the boundary value of x_2', see (B.15)

$$\boldsymbol{v}^{(1)}(\boldsymbol{x}, T) = \nabla\bigg[\frac{1}{8\pi^2\tilde{x}} \partial_{z_0} \ln\Big(|x_2' + \sqrt{(x_2')^2 + z_0^2 + (x_1^0)^2}|\Big)\bigg]\bigg|_{x_2' = \{x_2' : R_1|_{x_1' = x_1^0} = T\}} =$$

$$\nabla\bigg[\frac{1}{8\pi^2\tilde{x}} \partial_{z_0}\bigg(\ln\Big(\frac{T + \sqrt{T^2 - z_0^2 - (x_1^0)^2}}{T - \sqrt{T^2 - z_0^2 - (x_1^0)^2}}\Big) \mathrm{H}\big(T - c^{-1}\sqrt{z_0^2 + (x_1^0)^2}\big)\bigg)\bigg] \,. \tag{B.23}$$

Upon evaluating the derivative with respect to z_0, we obtain

$$\boldsymbol{v}^{(1)}(\boldsymbol{x}, T) = \nabla\bigg(\frac{z_0}{4\pi^2\tilde{x}^2} \frac{T(x_1^0 - \tilde{x})}{\big(T^2 - z_0^2 - (x_1^0)^2\big)_+^{1/2} \big(z_0^2 + (x_1^0)^2\big)} \bigg) \,, \tag{B.24}$$

where the generalized function in the denominator is the same as for the pressure (B.17), and can be rewritten as (B.19).

Appendix C The response field for case 2

To obtain the response for the control in case 2, we start to examine the characteristics of our transducers. The derivation in Appendix A–B is for the particle velocity normalization of the boundary condition, both for the control and for the measurement. If we instead of velocity normalization use the pressure normalization, then the boundary condition takes the form (*cf.* (6.14))

$$\frac{p + \mathcal{Y}^{-1} v_3}{2} = p_{+,\mathrm{N_P}}^{(2)} \,, \quad \text{and} \quad m_{(2)} = \frac{q - \mathcal{Y}^{-1} u_3}{2} \,. \tag{C.1}$$

The control operator is then expressed in terms of the eigenvector in the pressure normalization, *i.e.*, $\boldsymbol{\eta}^+$ in (A.4) is replaced by $\boldsymbol{\eta}_{(2)}^+$, where

$$\boldsymbol{\eta}_{(2)}^{\pm} = \begin{pmatrix} 1 \\ \pm s^{-1}\sqrt{s^2 + \tilde{\xi}^2} \end{pmatrix} \,. \tag{C.2}$$

Thus the symbol of the control operator, $\boldsymbol{w}^+_{(2)}$, in this normalization is

$$\begin{pmatrix} p \\ \tilde{\boldsymbol{v}} \\ v_3 \end{pmatrix} = (\boldsymbol{w}^+_{(2)} p^{(2)}_{+,\mathrm{N_p}})(\tilde{\boldsymbol{\xi}}, x_3, s) = \begin{pmatrix} -\partial_3 \\ s^{-1}\mathrm{i}\tilde{\boldsymbol{\xi}}\partial_3 \\ s^{-1}\partial_3^2 \end{pmatrix} \frac{\mathrm{e}^{-x_3\sqrt{s^2+\tilde{\xi}^2}}}{\sqrt{s^2+\tilde{\xi}^2}} p^{(2)}_{+,\mathrm{N_p}}(\tilde{\boldsymbol{\xi}}, s) \; . \tag{C.3}$$

Using (A.8), we obtain the control operator as

$$p(\boldsymbol{x}, T) = -\partial_3 \int_0^T \int_{\mathbb{R}^2} \frac{\delta(T - t' - |\boldsymbol{x} - \tilde{\boldsymbol{x}}'|)}{2\pi|\boldsymbol{x} - \tilde{\boldsymbol{x}}'|} p^{(2)}_{+,\mathrm{N_p}}(\tilde{\boldsymbol{x}}', t') \, \mathrm{d}x'_1 \, \mathrm{d}x'_2 \, \mathrm{d}t' \; , \tag{C.4}$$

and

$$\boldsymbol{v}(\boldsymbol{x}, T) = \nabla\partial_3 \int_0^T \int_{\mathbb{R}^2} \frac{\delta(T - t' - |\boldsymbol{x} - \tilde{\boldsymbol{x}}'|)}{2\pi|\boldsymbol{x} - \tilde{\boldsymbol{x}}'|} \int_0^{t'} p^{(2)}_{+,\mathrm{N_p}}(\tilde{\boldsymbol{x}}', t'') \, \mathrm{d}t'' \, \mathrm{d}x'_1 \, \mathrm{d}x'_2 \, \mathrm{d}t' \; . \tag{C.5}$$

Hence, the normalization of the boundary condition changes the field, as expected, *cf.* (6.18) and (6.19). The change related to the different transducer normalizations can be compared to solving a partial differential equation with Neumann and Dirichlet boundary condition respectively.

The field from the pressure pulse at the surface, $\{q, u_3\}$, in (6.24) is independent of normalization, but we measure particle velocity, see (C.1), thus in the pressure normalization the measured signal becomes

$$\begin{pmatrix} q(\tilde{\boldsymbol{\xi}}, 0, s) \\ u_3(\tilde{\boldsymbol{\xi}}, 0, s) \end{pmatrix} = \frac{s\mathrm{e}^{-z_0\sqrt{s^2+\tilde{\xi}^2}}}{2\sqrt{s^2+\tilde{\xi}^2}} \boldsymbol{\eta}^-_{(2)}(\tilde{\boldsymbol{\xi}}, s) \Rightarrow m_{(2)}(\tilde{\boldsymbol{\xi}}, s) = \frac{s\mathrm{e}^{-z_0\sqrt{s^2+\tilde{\xi}^2}}}{2\sqrt{s^2+\tilde{\xi}^2}} \; , \tag{C.6}$$

in the transform domain, and hence

$$m_{(2)}(\tilde{\boldsymbol{x}}, t) = \partial_t \frac{\delta(t - \sqrt{\tilde{x}^2 + z_0^2})}{4\pi\sqrt{\tilde{x}^2 + z_0^2}} \; . \tag{C.7}$$

Thus the control corresponding to the $m_{(2)}$ measurement is given by

$$p^{(2)}_{+,\mathrm{N_p}} = \mathrm{H}(t) m_{(2)}(\tilde{\boldsymbol{x}}, T - t) = -\mathrm{H}(t)\partial_t \frac{\delta(T - t - \sqrt{\tilde{x}^2 + z_0^2})}{4\pi\sqrt{\tilde{x}^2 + z_0^2}} \; . \tag{C.8}$$

We substitute the control (C.8) into (C.4) and (C.5) to obtain

$$p^{(2)}(\boldsymbol{x}, T) = \partial_3 z_0^{-1} \partial_{z_0} \int_{\mathbb{R}^2} \mathrm{H}(T - |\boldsymbol{x} - \tilde{\boldsymbol{x}}'|) \frac{\delta(|\boldsymbol{x} - \tilde{\boldsymbol{x}}'| - \sqrt{(\tilde{x}')^2 + z_0^2})}{8\pi^2|\boldsymbol{x} - \tilde{\boldsymbol{x}}'|} \, \mathrm{d}x'_1 \, \mathrm{d}x'_2 \; , \tag{C.9}$$

and

$$\begin{aligned} &\boldsymbol{v}^{(2)}(\boldsymbol{x}, T) = \\ &- \nabla\partial_3 z_0^{-1} \partial_{z_0} \int_{\mathbb{R}^2} \mathrm{H}\big(T - \sqrt{(\tilde{x}')^2 + z_0^2}\big) \frac{\mathrm{H}(\sqrt{(\tilde{x}')^2 + z_0^2} - |\boldsymbol{x} - \tilde{\boldsymbol{x}}'|)}{8\pi^2|\boldsymbol{x} - \tilde{\boldsymbol{x}}'|} \, \mathrm{d}x'_1 \, \mathrm{d}x'_2 \; . \end{aligned} \tag{C.10}$$

We rewrite (C.10) by evaluating ∂_{z_0}, thus

$$\boldsymbol{v}^{(2)}(\boldsymbol{x},T) = -\nabla\partial_3 \int_{\mathbb{R}^2} \mathrm{H}\Big(T - \sqrt{(\tilde{x}')^2 + z_0^2}\Big) \frac{\delta(\sqrt{(\tilde{x}')^2 + z_0^2} - |\boldsymbol{x} - \tilde{\boldsymbol{x}}'|)}{8\pi^2 |\boldsymbol{x} - \tilde{\boldsymbol{x}}'| \sqrt{(\tilde{x}')^2 + z_0^2}} - \delta\Big(T - \sqrt{(\tilde{x}')^2 + z_0^2}\Big) \frac{\mathrm{H}(\sqrt{(\tilde{x}')^2 + z_0^2} - |\boldsymbol{x} - \tilde{\boldsymbol{x}}'|)}{8\pi^2 |\boldsymbol{x} - \tilde{\boldsymbol{x}}'| \sqrt{(\tilde{x}')^2 + z_0^2}} \,\mathrm{d}x_1' \,\mathrm{d}x_2' \,. \quad \text{(C.11)}$$

The evaluation of (C.9) follows directly of its corresponding evaluation of the response in particle velocity normalization, see (B.8), we obtain

$$p^{(2)}(\boldsymbol{x},T) = \frac{-1}{4\pi^2 \tilde{x}^2} \partial_3 \frac{\tilde{x}^2 - x_3^2 + z_0^2}{\Big([T^2 - x_3^2 - \big(\tilde{x} - \sqrt{T^2 - z_0^2}\big)^2][\big(\tilde{x} + \sqrt{T^2 - z_0^2}\big)^2 + x_3^2 - T^2]\Big)_+^{1/2}} \,. \quad \text{(C.12)}$$

Appendix D The pressure response distribution for $T \to \infty$

In this section, we give the details for the calculation of the limit $T \to \infty$ of the pressure response (6.31) in case 1.

We rewrite the denominator of (6.31) in the more convenient form

$$p^{(1)}(\boldsymbol{x},T) = \frac{-z_0}{4\pi^2 x_3 \tilde{x}^2} \partial_3 \frac{\tilde{x}^2 - x_3^2 + z_0^2}{\Big([\big(\sqrt{T^2 - z_0^2} + \sqrt{T^2 - x_3^2}\big)^2 - \tilde{x}^2][\tilde{x}^2 - \big(\sqrt{T^2 - z_0^2} - \sqrt{T^2 - x_3^2}\big)^2]\Big)_+^{1/2}} \,. \quad \text{(D.1)}$$

In the limit $T \to \infty$, let $\phi = \phi(\tilde{\boldsymbol{x}}, x_3)$ be a compactly supported test function, *i.e.*, smooth and bounded. We require that

$$\text{supp } \phi \subset \{\boldsymbol{x} \in \mathbb{R}^3 : x_3 > 0\} \quad \text{and diam } \phi \le D_\phi \,, \quad \text{(D.2)}$$

for some fixed number $D_\phi > 0$. As we are only interested in the limit $T \to \infty$, we require that $T >> z_0$. Let us define the pressure functional $p_f = p_f(T)$ as

$$p_f = \int_{\mathbb{R}^3_+ \cap \text{supp } \phi} p^{(1)}(\boldsymbol{x},T) \phi(\tilde{\boldsymbol{x}}, x_3) \,\mathrm{d}x_1 \,\mathrm{d}x_2 \,\mathrm{d}x_3 \,. \quad \text{(D.3)}$$

By partial integration we push the derivative to the test function to obtain

$$p_f = \int_{\mathbb{R}^3_+ \cap \text{supp } \phi} \frac{z_0}{4\pi^2} \Big(\partial_3 \frac{\phi(\tilde{\boldsymbol{x}}, x_3)}{x_3}\Big) \frac{(\tilde{x}^2 - x_3^2 + z_0^2) \,\mathrm{d}x_1 \,\mathrm{d}x_2 \,\mathrm{d}x_3}{\tilde{x}^2 \Big([\big(\sqrt{T^2 - z_0^2} + \sqrt{T^2 - x_3^2}\big)^2 - \tilde{x}^2][\tilde{x}^2 - \big(\sqrt{T^2 - z_0^2} - \sqrt{T^2 - x_3^2}\big)^2]\Big)_+^{1/2}} \,. \quad \text{(D.4)}$$

We eliminate the appearance of T in the integrand with the change of variables

$$\check{z}_0 = \frac{z_0}{\sqrt{T^2 - z_0^2}} \,, \quad \check{x}_3 = \frac{x_3}{\sqrt{T^2 - z_0^2}} \,, \quad \check{r} = \frac{\tilde{x}}{\sqrt{T^2 - z_0^2}} \,, \tag{D.5}$$

giving $\mathrm{d}x_1\,\mathrm{d}x_2\,\mathrm{d}x_3 = (T^2 - z_0^2)^{3/2}\check{r}\,\mathrm{d}\check{r}\,\mathrm{d}\check{x}_3\,\mathrm{d}\theta$. With this change of variables the the denominator takes the form

$$(\dots)_+^{1/2} = \\ (T^2 - z_0^2)\left(\left[\left(1 + \sqrt{1 - \check{x}_3^2 + \check{z}_0^2}\right)^2 - \check{r}^2\right]\left[\check{r}^2 - \left(1 - \sqrt{1 - \check{x}_3^2 + \check{z}_0^2}\right)^2\right]\right)_+^{1/2} .$$

For notational convenience let

$$\psi(\check{r}\cos\theta, \check{r}\sin\theta, \check{x}_3, T) = \frac{\check{z}_0}{2\pi}\frac{\partial}{\partial \check{x}_3}\frac{\phi(\sqrt{T^2 - z_0^2}\check{r}\cos\theta, \sqrt{T^2 - z_0^2}\check{r}\sin\theta, \sqrt{T^2 - z_0^2}\check{x}_3)}{\check{x}_3} \,. \tag{D.6}$$

The limit of the integration, $\mathbb{R}^3_+ \cap \mathrm{supp}\ \phi$, in the new variables is included in the set

$$(\check{x}_3 - \check{z}_0)^2 + \check{r}^2 \leq \frac{D_\phi^2}{T^2 - z_0^2} \equiv \check{D}_\phi^2 \,, \tag{D.7}$$

for sufficiently large T. Hence, we only have to consider small $\check{r}$ and $|\check{x}_3 - \check{z}_0|$ as we make T arbitrary large. In particular, we can expand the test function ψ around $\check{r} = 0$, $\psi(\check{\boldsymbol{x}}, x_3) = \psi(0, 0, x_3, T) + \check{r}\psi_{\check{x}_1}\cos\theta + \check{r}\psi_{\check{x}_2}\sin\theta + \mathrm{O}(\check{r}^2)$. As the integrand, apart from the test function, is independent of θ, we obtain

$$p_f = \int_{\sqrt{(\check{x}_3 - \check{z}_0)^2 + \check{r}^2} \leq \check{D}_\phi} \big(\psi(0, 0, \check{x}_3, T) + \mathrm{O}(T^{-2})\big) \\ \frac{(\check{r}^2 - \check{x}_3^2 + \check{z}_0^2)\,\mathrm{d}\check{r}\,\mathrm{d}\check{x}_3}{\check{r}\Big(\big[\big(1 + \sqrt{1 - \check{x}_3^2 + \check{z}_0^2}\big)^2 - \check{r}^2\big]\big[\check{r}^2 - \big(1 - \sqrt{1 - \check{x}_3^2 + \check{z}_0^2}\big)^2\big]\Big)_+^{1/2}} \,. \tag{D.8}$$

The $\check{r}$-integral can be integrated exactly, but as we are only interested in the limit $T \to \infty$, we simplify the above expression as both $|\check{x}_3 - \check{z}_0|$ and $\check{r}$ are bounded above by $\check{D}_\phi = \mathrm{O}(T^{-1}) << 1$, for sufficiently large T. Applying Taylor expansion gives

$$1 + \sqrt{1 - \check{x}_3^2 + \check{z}_0^2} = 2 + \mathrm{O}(T^{-1}) \,, \quad 1 - \sqrt{1 - \check{x}_3^2 + \check{z}_0^2} = \frac{\check{x}_3^2 - \check{z}_0^2}{2} + \mathrm{O}(T^{-2}) \,, \tag{D.9}$$

hence

$$(\dots)_+^{1/2} = \big(\big[4\check{r}^2 - (\check{x}_3^2 - \check{z}_0^2)^2\big]\big)_+^{1/2} + \mathrm{O}(T^{-1}) \,. \tag{D.10}$$

Thus the pressure functional becomes

$$p_f = \int_{\sqrt{(\check{x}_3 - \check{z}_0)^2 + \check{r}^2} \leq \check{D}_\phi} \frac{\check{r}^2 - \check{x}_3^2 + \check{z}_0^2}{\check{r}\big[4\check{r}^2 - (\check{x}_3^2 - \check{z}_0^2)^2\big]_+^{1/2}}\psi(0, 0, \check{x}_3, T)\,\mathrm{d}\check{r}\,\mathrm{d}\check{x}_3 + \dots \,. \tag{D.11}$$

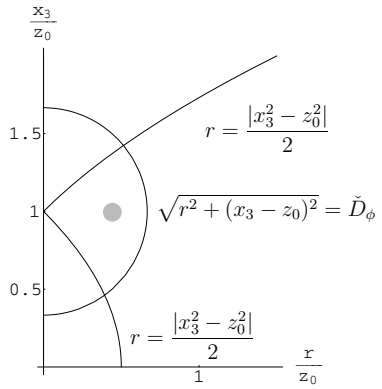

Figure 12: The triangle with the gray dot is the area of integration. The outer circle bounds the domain of ψ and the cutoff, $(...)_+^{1/2}$, is shown as the two lines entering the half-circle.

The disk $\sqrt{(\check{x}_3-\check{z}_0)^2+\check{r}^2}\le\check{D}_\phi$, together with the step function indicated by the plus sign on $(...)_+^{1/2}$ is depicted in Figure 12. With the change of variables

$$\check{r}=|\check{x}_3^2-\check{z}_0^2|u/2=\zeta u/2\;, \tag{D.12}$$

we find

$$p_f=\int_{|\check{x}_3-\check{z}_0|f(\check{x}_3)\le 2\check{D}_\phi}\int_1^{2\zeta^{-1}\sqrt{\check{D}_\phi^2-(\check{x}_3-\check{z}_0)^2}}\psi(0,0,\check{x}_3,T)\frac{\zeta^2u^2/4-\check{x}_3^2+\check{z}_0^2}{\zeta u(u^2-1)^{1/2}}\,\mathrm{d}u\,\mathrm{d}\check{x}_3+\dots\;,$$

where $f(\check{x}_3)=\sqrt{4+(\check{x}_3+\check{z}_0)^2}$. Upon integrating we have

$$p_f=-\int_{|\check{x}_3-\check{z}_0|f(\check{x}_3)\le 2\check{D}_\phi}\psi(0,0,\check{x}_3,T)\Big(\frac{(\check{x}_3^2-\check{z}_0^2)\pi}{2|\check{x}_3^2-\check{z}_0^2|}-\frac{1}{4}\sqrt{4\check{D}_\phi^2-4(\check{x}_3-\check{z}_0)^2-\zeta^2}-\frac{\check{x}_3^2-\check{z}_0^2}{\zeta}\arctan\big(\zeta(4\check{D}_\phi^2-(\check{x}_3-\check{z}_0)^2-\zeta^2)^{-1/2}\big)\Big)\,\mathrm{d}\check{x}_3+\dots$$

Observe that on the given interval we have the upper bound

$$\frac{1}{4}\sqrt{4\check{D}_\phi^2-4(\check{x}_3-\check{z}_0)^2-\zeta^2}\le\check{D}_\phi/2\;, \tag{D.13}$$

this together with that the square root is a continuous function, and that the test function is bounded above, gives that the integral of this term vanish as $T\to\infty$. For the arctan-term, we observe that it is continuous at $\check{x}_3=\check{z}_0$, since $\arctan\epsilon=\epsilon+\dots$, furthermore, on the given interval

$$\big|\mathrm{sgn}(\check{x}_3^2-\check{z}_0^2)\arctan\big(\zeta(4\check{D}_\phi^2-(\check{x}_3-\check{z}_0)^2-\zeta^2)^{-1/2}\big)\big|\le\frac{\pi}{2}\;, \tag{D.14}$$

thus, as the test function is bounded, this term also give a vanishing contribution to the integral.

With the above considerations the pressure functional becomes

$$p_f = -\frac{\pi}{2}\int_{|\check{x}_3-\check{z}_0|f(\check{x}_3)\leq 2\check{D}_\phi} \psi(0,0,\check{x}_3,T)\frac{\check{x}_3^2-\check{z}_0^2}{|\check{x}_3^2-\check{z}_0^2|}\,\mathrm{d}\check{x}_3 + \mathrm{O}(T^{-1})\ . \tag{D.15}$$

If we now substitute the expression for ψ, (D.6), we find that

$$p_f = -\frac{\check{z}_0}{4}\int_{|\check{x}_3-\check{z}_0|f(\check{x}_3)\leq 2\check{D}_\phi} \left(\partial_{\check{x}_3}\frac{\phi(0,\check{x}_3\sqrt{T^2-z_0^2})}{\check{x}_3}\right)\mathrm{sgn}(\check{x}_3^2-\check{z}_0^2)\,\mathrm{d}\check{x}_3 + \mathrm{O}(T^{-1})\ . \tag{D.16}$$

This integral is evaluated as

$$\begin{aligned} p_f &= \frac{\check{z}_0}{4}\int_{|\check{x}_3-\check{z}_0|f(\check{x}_3)\leq 2\check{D}_\phi} \phi(0,\check{x}_3\sqrt{T^2-z_0^2})\left(\check{x}_3^{-1}\partial_{\check{x}_3}\mathrm{sgn}(\check{x}_3^2-\check{z}_0^2)\right)\mathrm{d}\check{x}_3 + \mathrm{O}(T^{-1}) \\ &= \frac{1}{2}\phi(0,z_0) + \mathrm{O}(T^{-1})\ . \end{aligned} \tag{D.17}$$

In the integration we used that z_0 is always in the domain $|\check{x}_3-\check{z}_0|f(\check{x}_3)\leq 2\check{D}_\phi$, for sufficiently small $\check{D}_\phi$, or correspondingly for large enough T. In the limit $T\to\infty$ we find that the distribution reduce to a delta Dirac at $\tilde{\boldsymbol{x}}=0$ and $x_3=z_0$. Hence, in the limit we get back half original pressure pulse, in the pressure component.

References

[1] G. S. S. Ávila and D. G. Costa. Asymptotic properties of general symmetric hyperbolic systems. *Journal of Functional Physics*, **35**, 49–63, 1980.

[2] C. Bardos and M. Fink. Deterministic mathematical analysis of the time reversal mirror. `http://www.msri.org/publications/video/index03.html`, November 2001.

[3] C. Bardos, G. Lebeau, and J. Rauch. Sharp sufficient conditions for the observation, control, ans stabilization of waves from the boundary. *SIAM J. Control Optim.*, **30**(5), 1024–65, 1992.

[4] P. Blomgren, G. Papanicolaou, and H. Zhao. Super-resolution in time-reversal acoustics. *J. Acoust. Soc. Am.*, **111**, 230–248, 2002.

[5] D. Cassereau and M. Fink. Time-reversal of ultrasonic fields — part iii: Theory of the closed time-reversal cavity. *IEEE Trans. Ultrason., Ferroelec., Freq. Contr.*, **39**(5), 579–92, 1992.

[6] M. Cheney, D. Isaacson, and M. Lassas. Optimal acoustical measurements. *SIAM J. Appl. Math.*, **61**, 1628–47, 2001.

[7] M. Cheney and G. Kristensson. Optimal electromagnetic measurements. *J. Electromagn. Waves Appl.*, **15**(10), 1323–36, 2001.

[8] H. O. Cordes. *The Technique of Pseudodifferential Operators*. Number 202 in London Mathematical Society Lecture Notes Series. Cambridge University Press, Cambridge, 1995.

[9] A. Derode, P. Roux, and M. Fink. Robust acoustic time reversal with high-order multiple scattering. *Phys. Rev. Lett.*, **75**(23), 4206–09, December 1995.

[10] M. Fink and C. Prada. Acoustic time-reversal mirrors. *Inverse Problems*, **17**(1), R1–R38, 2001.

[11] M. Fink. Time-reversal mirrors. *J. Phys. D: Applied Phys.*, **26**, 1333–50, 1993.

[12] M. Fink. Time reversed acoustics. *Physics Today*, **3**, 34–40, March 1997.

[13] M. Fink. Time-reversed acoustics. *Scientific American*, **281**(5), 91–97, November 1999.

[14] M. Gustafsson. *Wave Splitting in Direct and Inverse Scattering Problems*. PhD thesis, Lund University, Lund, Sweden, 2000. `http://www.es.lth.se/home/mats/`.

[15] S. He, S. Ström, and V. H. Weston. *Time domain wave-splitting and inverse problems*. Oxford University Press, Oxford, 1998.

[16] M. V. de Hoop. Generalization of the Bremmer coupling series. *J. Math. Phys.*, **37**(7), 3246–82, 1996.

[17] B. L. G. Jonsson. *Directional Decomposition in Anisotropic Heterogeneous Media for Acoustic and Electromagnetic Fields*. PhD thesis, Royal Institute of Technology, Stockholm, Sweden, 2001.

[18] B. L. G. Jonsson and M. V. de Hoop. Wave field decomposition in anisotropic fluids. *Acta Appl. Math.*, **67**(2), 117–71, June 2001.

[19] H.-O. Kreiss and J. Lorenz. *Initial-Boundary Value Problems and the Navier-Stokes Equations*. Academic Press, San Diego, 1989.

[20] R. Leis. *Initial Boundary Value Problems in Mathematical Physics*. B. G. Teubner, Stuttgart, 1986.

[21] J. L. Lions. *Optimal Control of Systems Governed by Partial Differential Equations*, volume 170 of *Die Grundlehren der mathematischen Wissenschaften in Einzeldarstellungen mit besonderer Berücksichtigung der Anwendungsgebiete*. Springer-Verlag, Berlin, 1971.

[22] C. S. Morawetz. *Notes on time decay and scattering for some hyperbolic problems*, volume 19. SIAM, Philadelphia, 1975.

[23] P. M. Morse and H. Feshbach. *Methods of Theoretical Physics*, volume II. MacGraw-Hill, New York, 1953.

[24] A. W. Naylor and G. R. Sell. *Linear Operator Theory in Engineering and Science*. Springer-Verlag, New York, seccond edition, 1982.

[25] A. D. Pierce. *Acoustics: An Introduction to its Physical Principles and Applications*. Acoustical Society of America, New York, 1989.

[26] C. Prada, J.-L. Thomas, and M. Fink. The iterative time reversal process: Analysis of the convergence. *J. Acoust. Soc. Am.*, **97**, 62–71, 1995.

[27] A. P. Purdnikov, Y. A. Brychkov, and O. I. Marichev. *Integrals and Series vol. 2 Special Functions*. Gordon and Brech Science Publishers, London, 1986.

[28] Y. Saad. *Iterative Methods for Sparse Linear Systems*. PWS Publishing Company, Boston, 1996.

[29] M. A. Shubin. *Pseudodifferential Operators and Spectral Theory*. Springer Series in Soviet Mathematics. Springer-Verlag, Berlin, 1987.

[30] J. C. Strikwerda. *Finite Difference Schemes and Partial Differential Equations*. Chapman & Hall, New York, 1989.

[31] V. H. Weston. Factorization of the wave equation in higher dimensions. *J. of Math. Phys.*, **28**(5), 1061 – 68, 1987.

[32] V. H. Weston. Time-domain wave splitting of Maxwell's equations. *J. Math. Phys.*, **34**(4), 1370–92, 1993.